Non-modal vibration-based methods for Bridge Damage Identification

Rick M. Delgadillo[a]*, and Joan R. Casas[a]

[a]Department of Civil and Environmental Engineering, Technical University of Catalonia (BarcelonaTech), Catalonia, Spain

Campus Nord, C1 building. Jordi Girona, 1-3, 08034, Barcelona, Spain

e-mail. Rick M. Delgadillo: rick.milton.delgadillo@upc.edu. Joan R. Casas: joan.ramon.casas@upc.edu

ABSTRACT

Many methods of damage identification in bridge structures have focused on the use of either numerical models, modal parameters or non-destructive damage tests as a means of condition assessment. These techniques can often be very effective but can also suffer from specific pitfalls such as, numerical model calibration issues for nonlinear and inelastic behaviour, modal parameter sensitivity to environmental and operational conditions and bridge usage restrictions for non-destructive testing. The present paper covers alternative approaches to damage identification of bridge structures using empirical parameters applied to measured vibration response data obtained from two field experiments of progressively damaged bridges subjected to ambient and vehicle induced excitation, respectively. Numerous non-modal vibration-based damage features are detailed and selected for the assessment of either the ambient or vehicle induced excitation data based on their inherent properties. The results of the application to 2 real bridges, one under ambient vibration and the other of forced vibration demonstrate the robustness of the proposed damage features for damage identification using measurements of ambient and vehicle excitations. Moreover, this investigation has demonstrated that the novel empirical vibration parameters assessed are suitable for damage detection, localization and quantification.

Keywords: SHM, vibration parameters, damage identification, Hilbert Huang Transform, ambient excitation, forced vibration.

LIST OF NOTATIONS

CAV   Cumulative absolute velocity

CAD   Cumulative absolute displacement

DVI   Distributed vibration intensity

MCVI   Mean cumulative vibration intensity

IVI   Instantaneous vibration intensity

AIVI   Amalgamated instantaneous vibration intensity

EMD   Empirical mode decomposition

ICEEMDAN Improved complete ensemble empirical mode decomposition with
adaptive noise

HHT   Hilbert-Huang Transform

IMF   Intrinsic mode functions

MCD   Minimum covariance determinate

MSD   Mahalanobis squared distance

MTS   Mahalanobis Taguchi System

1 INTRODUCTION

Structural damage and degradation of bridges is dangerous and costly occurrence. Once

identified, repair works should be carried out promptly, as maintenance costs dramatically

increase when damage is left unattended; therefore, it is vital that bridge owners conduct

necessary visual inspections and structural integrity testing on a regular basis. However,

due to the large quantity of bridges in the network, this is impractical. Instead of directly inspecting every bridge, sensors can be used to indirectly infer the presence of damage using theoretical relationships, such as that of modal frequency and stiffness. Numerous modal parameters have been proposed in this sense, some of which are presented and discussed in (Moughty & Casas, 2017). However, also other non-modal parameters have been considered. The majority of them are found and discussed in Kramer (1996), such as RMS acceleration, Arias Intensity, Cumulative Absolute Velocity (CAV) and others. In general, these parameters were defined to represent the frequency content, amplitude or duration of a ground motion, Nonetheless, nowadays they can be used to detect damages in real civil structures obtaining successful outcomes, as seen later in the present paper.

In this context, Kim et al. (2013) utilized conventional dynamic properties as a damage-sensitivity derived from linear system parameters of a time series model. They found MTS (Mahalanobis Taguchi System) is able to enhance the identification of structural changes due to damage. (Goi & Kim, 2017) proposed a novel damage indicator automatically derived from a set of multivariate autoregressive models on an actual steel truss bridge. This damage indicator demonstrated that the modal information included in a multivariate system could help to improve damage detection performance. (Zhou et al., 2015) carried out a real experiment on a free-free steel beam excited by a shaker (structural forced dynamic response data). Mahalanobis Square Distance (MSD) approach was developed in order to detect the damage levels. The authors claimed that the MSD is effective for damage detection using frequency-based raw data. Additionally, this approach may function in operational conditions. (Nguyen et al., 2014b) improved Mahalanobis Square Distance method with a controlled data generation scheme based on

Monte Carlo simulation methodology. The effectiveness was demonstrated using a benchmark structure data from a building model with several damage levels.

The use of modal parameters as damage sensitive features have found that their performance may suffer from their sensitivity to environmental and operational conditions which can mask damage events. Additionally, the non-stationarity of some vibration signals creates a problem when using standard modal techniques based on Fourier transforms, as linear stationarity is assumed. Finally, Table 1 gives some advantages and disadvantages of the techniques applied to modal parameters in order to detect damages in real civil structures.

Table 1. Advantages and Disadvantages of damage detection methods based on modal parameters

Method	Advantages	Disadvantages	Reference
Mahalanobis Taguchi System (MTS)	serve to emphasize change of the damage-sensitive feature due to damage	An expert judgment is needed to select the initial parameters	(Kim et al., 2013)
Mahalanobis Square Distance (MSD)	Its simplicity and computational efficiency	MSD fails when nonlinearities are present in observations	(Zhou et al., 2015)
Autoregressive models	Can be used to extract damage-sensitive features	The appropriate order estimation of an AR model is a complex issue	(Laory et al., 2013) (Goi & Kim, 2017)
MSD with Minimum Covariance Determinate (MCD)	Produces high resolution of structural condition variation and reduce uncertainty regarding external sources of excitation	Do not present a computational efficiency since this process takes multiple iterations	(Moughty & Casas, 2017)

In applications not using modal parameters, and instead using displacement/strain measurements as features for damage identification, (Tondreau & Deraemaeker, 2014) proposed a damage sensitive feature in two experimental applications using ambient dynamic strain measurements. In this case, all the damage scenarios were correctly located without false alarms. (Sun et al., 2016) proposed a damage detection method by

analysing dynamic displacement of bridge structures under moving vehicle, which is represented by the numerical simulation of a beam model. The results showed both reliability and efficacy of this method in damage detection of bridge structures. Also, according to statistical hypothesis testing criteria, (Ou et al., 2017) covered a problem focused on the damage detection via the use of statistical and modal damage detection methods for a small-scale wind turbine. In conclusion, the statistical-based methods outperform modal-based ones, succeeding in the detection of induced damage, and they can be very well integrated into maintenance processes. (Fassois and Kopsaftopoulos, 2013) outlined several statistical time series methods for vibration based structural health monitoring using a laboratory truss structure. The proposed methods achieved the detection, the location and the quantification of damages. However, they were limited by the specific type of model employed and for the adequate user experience. Moreover, (Kankanamge & Dhanapala, 2016) utilized the wavelet analysis for identification of modal properties and damage detection in two case studies: a single-span steel girder bridge in Holland, Michigan and a cable-stayed bridge in mainland China. The results showed that Continuous Wavelet Transform (CWT) method is a very effective tool, which is able to provide reliable results both in modal parameters identification and damage detection. (Ding and Chen, 2013) analysed the multi-scale wavelet transform coefficients of curvatures of mode shapes in order to indicates the damage location in a simply supported beam bridge. The results showed that the peaks of the wavelet transform coefficients indicate the damage location. (Hester & Gonzalez, 2012) utilized the wavelet energy content to detect damage in a simply supported bridge beam model, which proved to be more sensitive to damage. The recent advances in Artificial Intelligence based damage identification methods are increasingly being used for their great performance. For instance, (Laory et al., 2013) proposed a methodology for damage detection that

combines moving principal component analysis (MPCA) with four regression-analysis methods applied in three case studies. The results indicate that the combined methods perform better than each individual method in terms of damage detectability and time to detection. (Nguyen et al., 2014a) used several variants of Principal Component Analysis (PCA) for detection and localization of damage on the Champangshiehl bridge and the precast panels. The results demonstrated that the damages were better distinguished in both cases.

Some researchers have applied other innovative techniques for analysis of bridge vibration data and damage identification. For instance, (Santos et al., 2013) implemented a strategy to detect structural damage using a symbolic data analysis in order to reduce raw vibration data through a statistical process utilizing Interquartile Ranges. The researchers obtained good results from the baseline-free strategy proposed, and this allowed to detect the structural changes regardless the modal quantities used (modal parameters) in real-time (without resorting to the entire data set).

The present paper, which is an extended version of the paper by Moughty and Casas, 2018b, details a number of empirical vibration parameters designed to be suitably applicable as damage indicator features to the specific vibration signals that are typical from either; long duration, low energy stationary ambient vibration or short duration, high energy non-stationary vehicle induced signals.

2 EMPIRICAL VIBRATION PARAMETERS

2.1 Vibration Parameters

The present section introduces the five vibration parameters that are extracted from acceleration responses that will be tested as vibration-based damage features.

(1) Cumulative Absolute Velocity (CAV)

Is an energy based vibration parameter proposed by Kramer (1996). It is the summed integral of all absolute acceleration values of the vibration response history as per Equation (1). In reality, this parameter represents the area under the absolute accelerogram and CAV presents a good correlation with structural damage potential. Figure 1 (a) and (b) show an tical acceleration record and the corresponding values of CAV as they evolve over time.

$$CAV = \int_0^t |\ddot{x}(t)| \, dt \tag{1}$$

(2) Cumulative Absolute Displacement (CAD)

Is an adaptation to the above CAV vibration parameter, however in this case the acceleration signal is first transformed into displacements using integration and band-pass filtering to avoid drift. Figure 1 (c) shows the CAD integral in the evaluated time:

$$CAD = \int_0^t |x(t)| \, dt \tag{2}$$
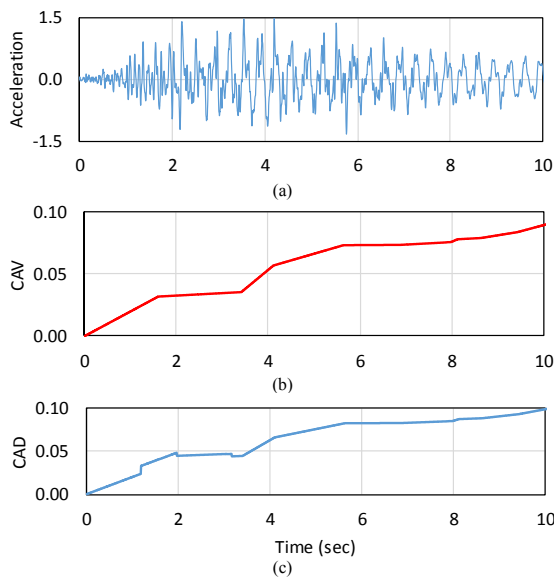
Figure 1. Illustration of the definitions of vibration parameters (a) acceleration time series (b) CAV (c) CAD.

(3) Distributed Vibration Intensity (DVI)

Is a novel vibration parameter that is based on the concept of vibration intensity, which in simple harmonic motion context can be defined as $(I=a^2/f)$, where a is acceleration amplitude and f is frequency. The SI units of vibration intensity are mm^2/s^3 and its logarithmic power form is decibels (dB). For the distributed variant employed herein, a Fourier transformation is applied to the vibration data and the summation of the vibration intensity values is taken within a frequency range, denoted by (f_i) within the limits m-n in Equation (3). It is important that the frequency range selected encompasses the first few modes of vibration of the structure; in the present study, the frequency range is taken as $(m$-$n = 1Hz – 20Hz)$. In this way, DVI may capture the damage sensitivity associated with energy and modal frequency changes.

$$DVI = \sum_{i=m}^{n} 10 log_{10} \left(\frac{\ddot{x}_i^2 \cdot (f_i)}{f_i} / I_S \right) \tag{3}$$

For $m \leq f_i \leq n$ (in Hz)

$$I_S = 10 mm^2 / s^3$$

(4) Mean Cumulative Vibration Intensity (MCVI)

First presented herein, is the second of three parameters based on the concept of vibration intensity (energy / frequency). In MCVI, the energy portion, i.e. the numerator, is the square of the aforementioned vibration parameter CAV, while the denominator is a weighted mean value of Fourier frequency within a specified frequency range. As per Equation (4), the weighting is applied to the discrete frequencies (f_i) via their corresponding Fourier Amplitude values (FA).

As highlighted for DVI, it is important that the frequency range selected encompasses the first few modes of vibration of the structure; in the present study, the frequency range is taken as *(m-n = 1Hz – 20Hz)*.

$$MCVI = \frac{\int_0^t \ddot{x}(\mathrm{t})^2 dt}{\left(\sum_{i=m}^{n} FA_i^2 .(f_i) \middle/ \sum_{i=m}^{n} FA_i^2 \right)} \tag{4}$$

For $m \le f_i \le n$ (in Hz)

(5) Instantaneous Vibration Intensity (IVI)

Is the last vibration parameter that is based on concept of vibration intensity (energy / frequency), however, in this case the vibration parameter is designed for use on non-stationary and non-linear data, such as the vehicle induced excitation case assessed in the present study. IVI is the product of two Hilbert-Huang Transform (HHT) (Huang et al., 1998) parameters; instantaneous amplitude and instantaneous frequency, which are commonly presented together in a Hilbert-Huang Spectrum. However, this method of representation is not easily quantifiable. A more objective representation of instantaneous amplitude and frequency can be obtained via IVI, whose calculation is summarized in following explanatory paragraphs. For a more in-depth explanation on IVI's calculation and application, the reader is referred to (Moughty & Casas, 2018a).

The first step is to decompose the raw non-stationary and non-linear vibrations signals into different Intrinsic Mode Functions (IMFs) using Empirical Mode Decomposition (EMD). In the present study, an advanced method of EMD is used to improve the acquisition performance of IMF, known as Improved Complete Ensemble Empirical Mode Decomposition with Adaptive Noise (ICEEMDAN) and proposed by (Colominas et al., 2014). The authors proposed substantial improvements to obtain

components with less noise and more physical meaning. The resulting IMFs $\{c_i(\tau)\}$ are

input into the Hilbert Transform:

$$H[c_i(t)] = \frac{1}{\pi} \int_{-\alpha}^{\alpha} \frac{c_i(\tau)}{t-\tau} d\tau \tag{5}$$

The resulting Hilbert Transform $H[c_i(t)]$ is grouped with $\{c_i(\tau)\}$ to form an

analytic signal $z(t)$ (Equation 6) whose constituents $a_i(t)$ and $\theta_i(t)$ (instantaneous

amplitudes and phases), can be expressed by Equation (7) & Equation (8) respectively.

Instantaneous frequencies $\{\varpi_i(t)\}$ of each IMF are determined by differentiating the

instantaneous phase function in Equation (9). Equation (10) expresses how the vibration

parameter IVI is obtained by combining the instantaneous amplitudes and frequencies.

Finally, note that IVI can be obtained for each particular sensor. Therefore, in order to

guarantee that all obtained physically meaningful IMFs are utilized for damage

localization, the sensor obtained IVIs can be combined to provide the Amalgamated

Instantaneous Vibration Intensity (AIVI), which is studied in more detail in the results

section.

$$z(t) = c_i(t) + jH[c_i(t)] = a_i(t) e^{j\theta_i(t)} \tag{6}$$

$$a_i(t) = \sqrt{c_i^2(t) + H^2[c_i(t)]} \tag{7}$$

$$\theta_i(t) = \arctan(\frac{H[c_i(t)]}{c_i(t)}) \tag{8}$$

$$\varpi_i(t) = \frac{d\theta_i(t)}{dt} \tag{9}$$

$$IVI_i(t) = a_i^2(t)/\varpi_i(t) \tag{10}$$

2.2 Application Suitability of Vibration Parameters

The variables of each bridge monitoring campaign, such as monitoring duration, excitation method, number and type of sensors can differ widely from project to project. This may be due to the influence of external conditions associated with each bridge, such as the traffic volume and type, socioeconomic factors and the financial budget available. The result being that the vibration data obtained may attain different properties that may render some damage sensitive features, such as those presented here, unsuitable for application. For instance, long duration vibration data may not be suitable for the vibration parameter IVI, as the computation effort of the EMD process would be substantial. Furthermore, Fourier-based damage sensitive features, such as modal parameters are unsuitable for non-stationary vibration data that would be typical of vehicle induced excitation bridge testing. The proposed methods studied here were applied when the traffic was closed, that is, when there was no normal traffic excitation. In addition, these methods are useful when there is only environmental vibration and for a controlled load test. For this reason, Table 2 is provided to give a breakdown of the applicability of each of the selected vibration parameters to specific vibration properties that may influence their damage identification performance.

Table 2. Vibration parameter application classification

Vib. Para. / Property	CAV	CAD	DVI	MCVI	IVI/AIVI
Fourier-Based Parameter	✗	✗	✓	✓	✗
Non-Stationary Signal Applicability	✓	✓	✗	✗	✓
Long Duration Signal Applicability	✓	✗	✓	✓	✗
Suitability to Ambient Induced Excitation	✓	✗	✓	✓	✗
Suitability to Vehicle Induced Excitation	✓	✓	✗	✗	✓

3 DAMAGE IDENTIFICATION METHOD

The damage identification methodology employed is dependent on the quantity of extracted vibration parameters and their origin. For instance, in an ambient condition test data, vibration parameters are continuously extracted every minute over the duration of the progressive damage test, while for a vehicle induced excitation test, vibration parameters are extracted for each vehicle crossing only. This provides two very differently sized datasets. In the vehicle induced excitation case, the method of damage detection is simple like-for-like comparison, while ambient excitation case requires the application of an outlier detection algorithm suited to the probability distribution of each vibration parameter. For Gaussian distributed vibration parameters, such as DVI and MCVI, the Mahalanobis Squared-Distance (MSD) multivariate outlier detection algorithm is employed. It uses mean and covariance data to train and assess dataset continuity. MSD is determined as shown in Equation (11), where $\{X\}_\varsigma$ is the potential outlier, $\{\overline{X}\}$ is the mean of the training data and $[\Sigma]$ is the covariance matrix of the training data.

$$D_\varsigma = (\{\overline{X}\}_\varsigma - \{X\})^T [\Sigma]^{-1} (\{X\}_\varsigma - \{\overline{X}\}) \tag{11}$$

In addition to the MSD, the Minimum Covariance Determinate (MCD) estimator is also employed to enhance robustness and reduce uncertainty regarding sources of ambient excitation by identifying and removing outliers from the training data prior to MSD. The FAST MCD algorithm by (Rousseeuw & Van Driessen, 1999) is employed in the present study.

For non-Gaussian distributed vibration parameters such as the energy-based parameter CAV, its value can never be less than zero and has no theoretical maximum. As such, it distribution fit can be taken as Log-Normal, which is unsuitable for use with

MSD. Instead, symbolic data objects are obtained from the Log-Normal distributions of overlapping windowed CAV datasets of 30min duration with 6 min overlap. Symbolic data objects are representative values of a larger data set that can be used in an SHM context, as demonstrated by Santos et al. (2013). In the present study, the overlapping Log-Normal distributions of CAV are reduced to their symbolic data objects of; Median and Interquartile Range. Using these two symbolic objects as a two dimensional damage feature vector, changes to the CAV distribution can be calculated using pairwise Euclidean distance as per Equation (12), where X_{UD} and X_{Dam} represent the first symbolic data object for the undamaged and damaged cases, respectively, and Y_{UD} and Y_{Dam} represent the second symbolic data object for the undamaged and damaged cases, respectively.

$$E.dist = \sqrt{\left(X_{UD} - X_{Dam}\right)^2 + \left(Y_{UD} - Y_{Dam}\right)^2} \qquad (12)$$

The damage identification method used in the case of the forced vibration is based on the Improved Complete Ensemble Empirical Mode Decomposition with Adaptive Noise (ICEEMDAN) as presented in Moughty and Casas 2018a.

4 CASE STUDIES

4.1 Ambient Excitation - S101 Bridge

The S101 was a post-tensioned concrete bridge located near Vienna in Austria that had a main span of 32m and two 12m side spans. The deck cross-section was 7.2m wide double-webbed t-beam, whose webs had a width of 0.6 m. The height of the beam varied from 0.9 m in the mid-span to 1.7 m over the piers, as can be seen in Figure 2. The columns, beams and the deck slab were built with concrete material of 2400 kg/m^3 density and the Young's modulus of 24.8 GPa. In 2008, it was decided to replace the S101 Bridge due to

insufficient carrying capacity and deteriorating structural condition being identified from visual inspection data. Before demolition, a progressive damage test was conducted on the S101 Bridge across 3 days in 2008 though the completion of a number of sequential actions, which are presented in Table 3. Overall, the damage applied can be divided into two main stages; (1) simulated pier foundation settlement, (2) bridge deck stiffness loss through the severing of four pre-stressed tendons. During the test the bridge was closed to traffic, meaning that excitation was mainly ambient, although one traffic lane beneath the bridge was kept in use. As for environment sources of excitation, very little temperature variation was observed throughout the test duration as sub-zero temperatures were kept within a 3 to 4 degree range due to persistent heavy cloud cover (VCE, 2009). Vibration data was recorded by 13 accelerometers located on one side of the bridge deck, with a sample rate of 500 Hz. Vibration recordings from the sensors did not cease throughout the progressive damage test. For the present study, the measured data was discretized into 66 sec long segments of 33,000 samples.

Figure 2. View of the S101 Bridge and bridge dimension (dimensions in centimeters)

Table 3. Damage actions applied to the S101 Bridge

Damage State	Damage Actions

1	Undamaged
2	North-Western (NW) pier cut through
3	NW pier lowered by 1cm
4	NW pier lowered by 2cm
5	NW pier lowered by 3cm
6	Support plates inserted & pier returned to origin
7	First pre-stressed tendon cut over NW pier
8	Second pre-stressed tendon cut over NW pier
9	Third pre-stressed tendon cut over NW pier
10	Forth pre-stressed tendon cut over NW pier

4.2 Vehicle-Induced Excitation - Steel Truss Bridge

The data have been obtained from a progressive damage test conducted on a Japanese bridge that was subjected to a moving vehicle excitation (Kim et al., 2013). The bridge in question was a simply-supported steel truss bridge that spanned 59.2m with a width of 3.6m and a max height of 8m. In the bridge, the truss members were built by beam elements and were assigned with steel material properties (density 7900 kg/m^3 and Young's modulus 200 GPa). Likewise, the deck was built of concrete material with the density 2400 kg/m^3 and elasticity modulus of 21 GPa. It was scheduled to be replaced in 2012, before which a progressive damage test was carried out while the bridge was closed to the public. Dynamic response was recorded from 8 uniaxial accelerometers, positioned as per Figure 3(b) and measuring the vertical acceleration, with sample rates of 200Hz. The induced damage scenarios consist of severing vertical members of the truss structure in the locations presented in Figure 3(b). The progression of the damage states is described in Table 4 and presented in Figure 4. The damage actions began with the partial intersection of the mid-span vertical member (DMG1), before its full intersection was completed (DMG2). After which, the damaged member was reconnected (RCV) with a welded flange. Finally, the vertical member at 5/8th span was completed severed (DMG3).
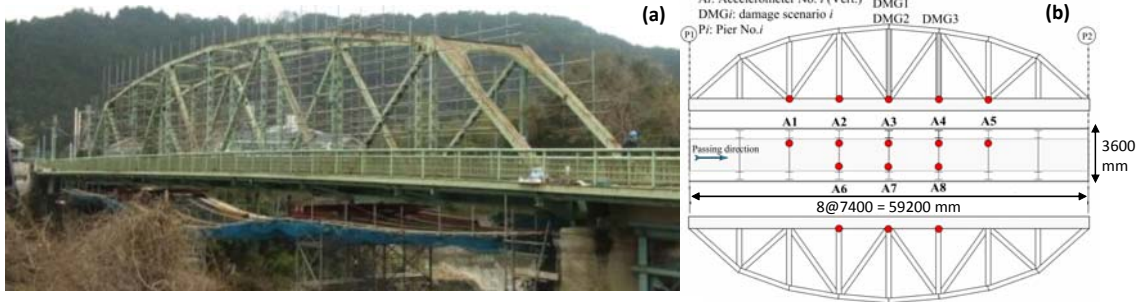
Figure 3. Steel truss bridge (a); sensor & damage locations (b)

Table 4. Damage actions conducted on the Steel Truss Bridge

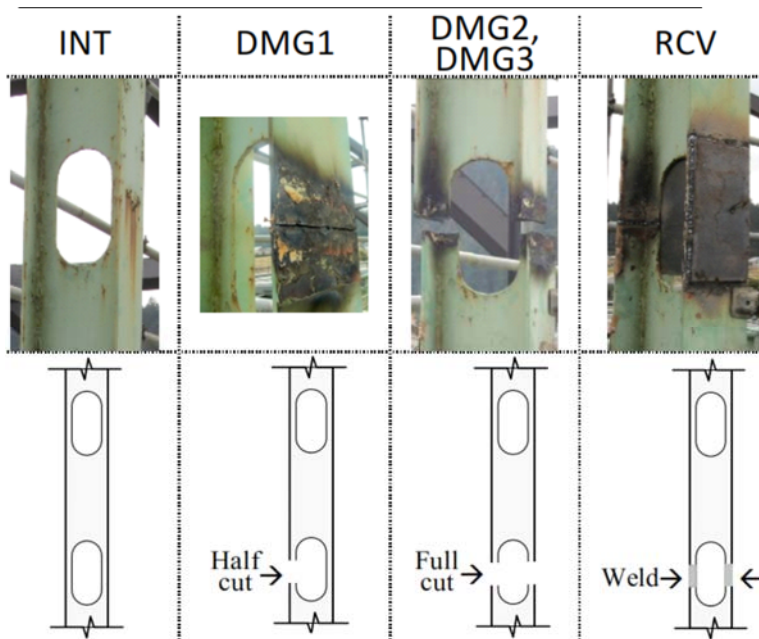| Damage State	Description of Damage Actions
1	Undamaged
2	Half cut in vertical member at mid-span
3	Full cut in vertical member at mid-span
4	Mid-span member reconnected
5	Full cut in vertical member at 5/8th span

Figure 4. Steel truss bridge damage scenarios

For each damage scenario, a 21kN double-axle truck crossed the bridge 3 times at approximately 40km/h. The weight of the vehicle was enough to excite the bridge and to obtain the vibration parameters. In addition, each damage scenario could be carried out

normally considering that the 21kN was not excessive. A sample time-history of acceleration response is presented in Figure 5 with the section of forced vibration shaded in grey. The forced vibration response is quite short in duration and highly non-stationary, as such it is unsuitable for Fourier-based transformation, therefore, this section of the signal is taken as the input for the parameter IVI.
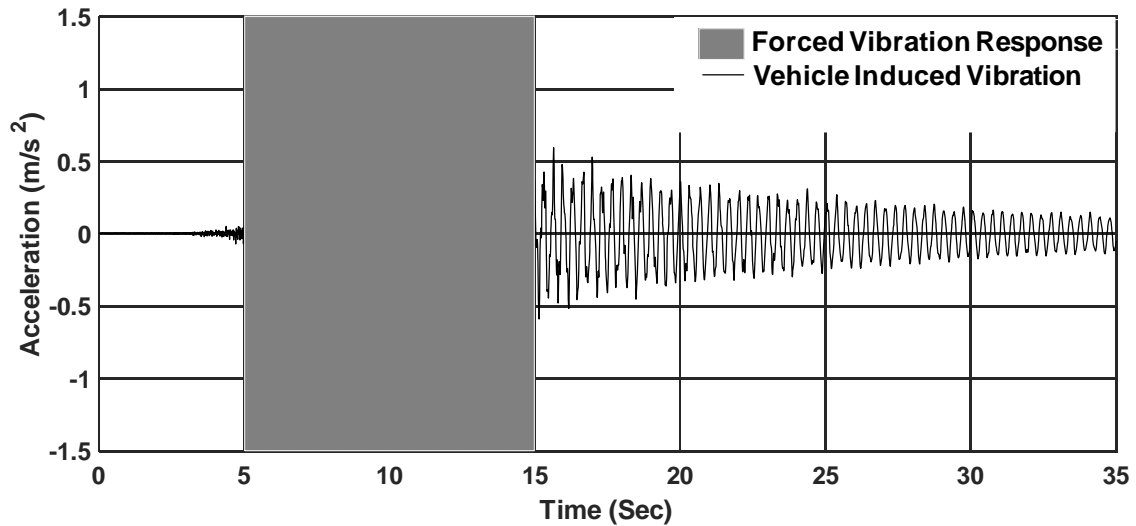
Figure 5. Example of vehicle induced vibration response

5 RESULTS

5.1 Ambient Excitation - S101 Bridge

The damage identification assessment results for the S101 Bridge under ambient excitation are presented herein for the three vibration parameters that were deemed suitably applicable to such conditions as per the criteria set out in Table 2.

   (1) CAV

The Euclidean Distance evolution of the CAV-based symbolic data objects (Median & Interquartile Range) throughout the duration of the progressive damage test is presented in Figure 6. For this purpose, all the damage scenarios presented in Table 3 were evaluated considering the Y-axis as a linear representation of time. It can be observed that an

enhanced divergence from the undamaged state occurs at the sensors located at the damaged North Pier during the pier settlement test. After the pier is returned to its original positions, the Euclidean distance returns close to normal. This is to be expected, as the pre-stressed tendons should supply enough compression to close the majority of cracks caused by the pier settlement, effectively reversing the simulated damage. The succeeding damage events that entail the severing of 4 pre-stressed tendons generate little change in CAV distribution through time. Although this may seem like a missed damage event, it may also indicate that a sufficient level of compression is still present in the remaining pre-stressed tendons to maintain normal structural behaviour without severely cracked sections.
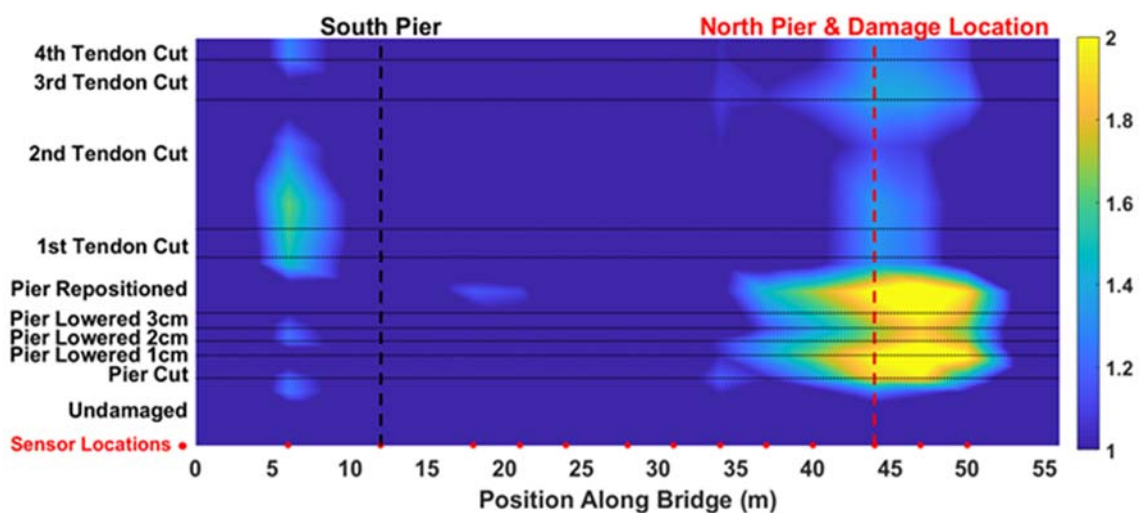
Figure 6. Evolution of CAV through time at each sensor using the Euclidian Distance of the chosen symbolic data objects of median and interquartile range of overlapping windowed CAV Lognormal distributions.

(2) DVI

The MSD evolution of the vibration parameter DVI throughout the duration of the progressive damage test is presented in Figure 7. It can be observed that an enhanced divergence from the undamaged state occurs across the bridge during the pier settlement test, but particularly so at the sensors located at the damaged North Pier. Similarly to

CAV, the divergence of CAD reduces upon pier repositioning, however, as the pre-stressed tendons are severed, damage is once again highlighted at the North Pier.
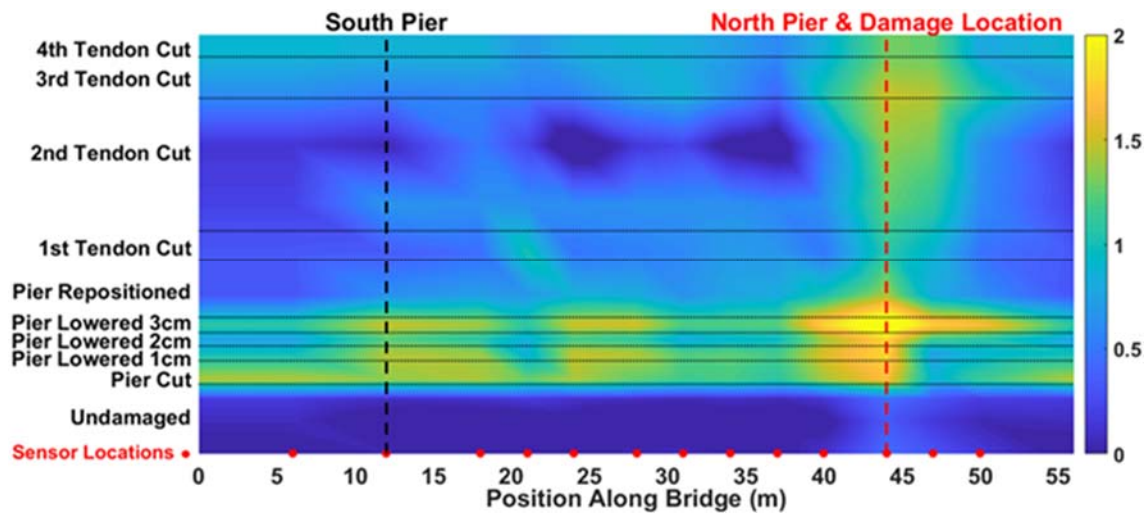
Figure 7. Evolution of DVI through time at each sensor using Mahalanobis Squared Distance.

(3) MCVI

The MSD evolution of the vibration parameter MCVI throughout the duration of the progressive damage test is presented in Figure 8. It can be observed that an enhanced divergence from the undamaged state occurs on the North side of the bridge during the pier settlement test, with no exact location of damage identified. For the severed pre-stressed tendons, MCVI provides a strong indication of damage for the 3rd tendon cut, but no others.
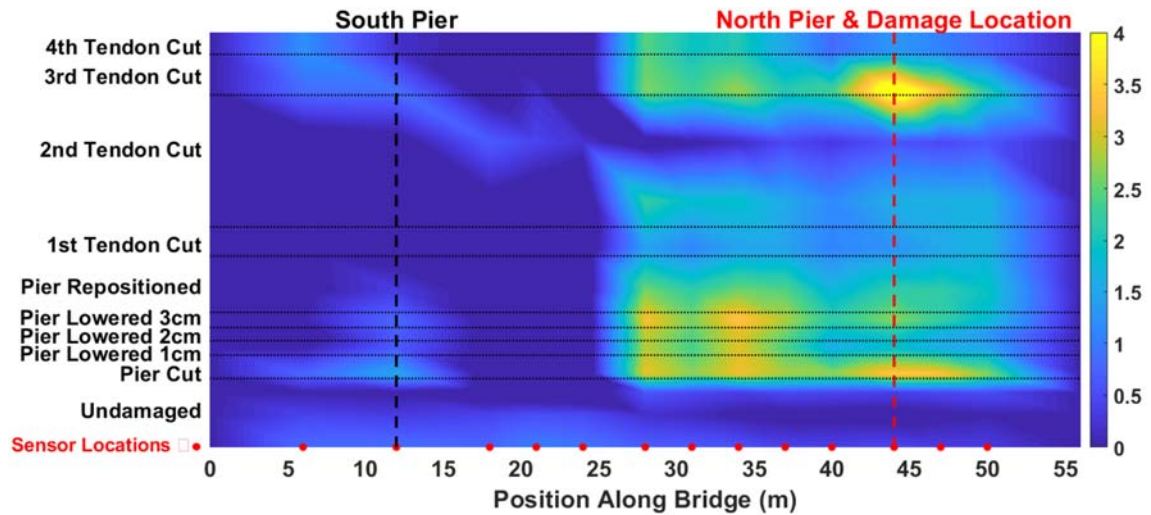
Figure 8. Evolution of MCVI through time at each sensor using Mahalanobis Squared Distance.

5.2 Vehicle-Induced Excitation – Steel Truss Bridge

In this section, an exhaustive analysis of Instantaneous Vibration Intensity parameter (IVI) is developed. IVI utilizes the time-frequency-energy representation of the well-known Hilbert Spectrum in a novel manner that provides more quantifiable measure of signal variations. In this study, the IVI's obtained for each vehicle crossing are analysed across a 10s duration that captures the forced vibration response of the bridge under the vehicle load (see case study number 2). For the undamaged condition, Figure 9 shows an example of Hilbert-Huang Spectrum that is obtained for the first 3 IMFs of Sensor 1 in the steel truss bridge described in the case of study. The time–frequency variation shows energy concentration around 3Hz, 6.8Hz and 13.3Hz, which represent the first, second and fifth vibrational mode as per Kim, et al. (2014). However, considering only this information is difficult to ascertain changes in structural behaviour. For this reason, a more quantitative representation known as IVI is presented in Figure 10. This relation obtained from Equation (10) considers both instantaneous frequencies and amplitudes.
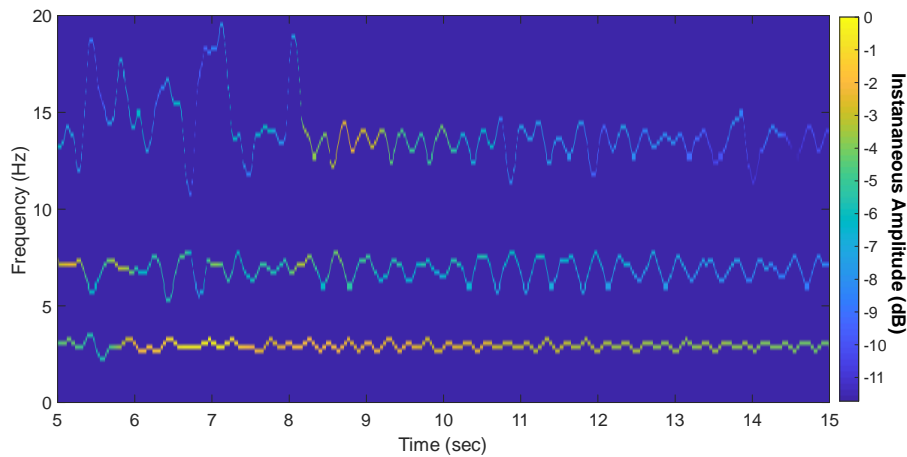
Figure 9. Hilbert-Huang Spectrum for first 3 IMFs
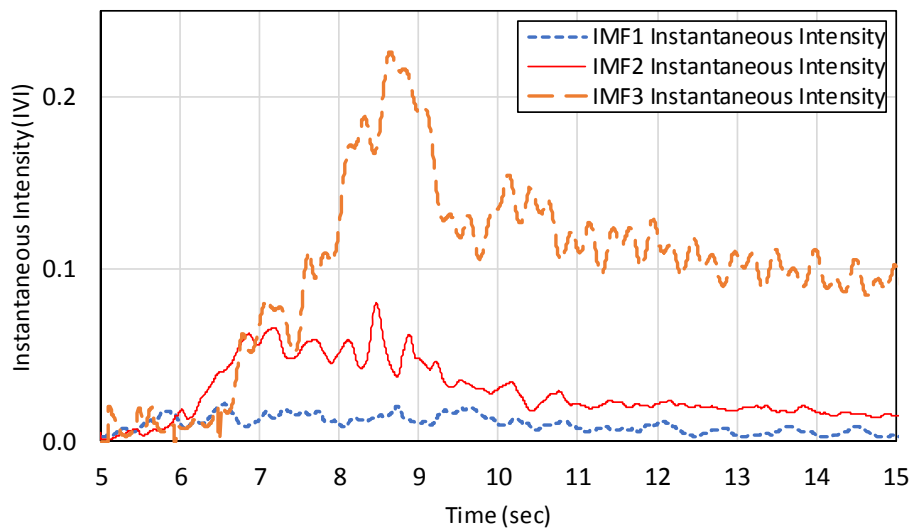
Figure 10. Instantaneous Vibration Intensity from first 3 IMFs

Previous studies presented by (Moughty & Casas, 2017) and (Moughty & Casas, 2018a) show that some IMFs extracted from the acceleration data are physically meaningful. For this purpose, it must be taken into account that three of the IMFs extracted from the tests that will be used here, correspond to the three natural vibration frequencies of the bridge and, therefore they are related to the IVI parameter.

5.2.1 Analysis based on individual IMF´s

As in this case each analyzed IMF corresponds to a natural frequency of the bridge, the analysis starts with the results obtained for each IMF separately. In this sense, Figure 11 shows the changes of IVI at each sensor along the bridge for frequency 1 (IMF 3) and

bearing in mind that the intensity increases as greater damage occurs since the IVI parameter is closely related to the amplitude and frequency. Figures 11 (a) to Figure 11 (e) display an interesting behavior for the first five sensors along the bridge, and it is clearly shown that the closer the sensor to the location where damage occurs, the better the sensor manages to capture the behavior of the bridge structure from an undamaged state, moderate damage (DMG 2), recovery (RCV) and severe damage (DMG 3). Furthermore, in location of critical sensors as 3 and 4, the Figure 11 (c) and Figure 11 (d) plot a greater increase of IVI and a shift to the left due damage 2 and damage 3 respectively. Additionally, the analysis of the maximum peaks shows a considerable increase of $\Delta 1=0.08$ and $\Delta 2=0.13$ between the un-damaged and damaged scenarios, which demonstrate the presence of damage close to them. On the other hand, sensors 7 and 8 located on the other side of the cross section of the bridge show slight variation between un-damaged and damaged cases ($\Delta 3=0.03$ and $\Delta 4=0.03$), which means that they can not detect damage because the damage is not close to them, as can be shown in Figure 11 (g) and Figure 11 (h) respectively. In addition, the sensor 6 do not show different behavior between un-damaged and damaged cases (Figure 11f).
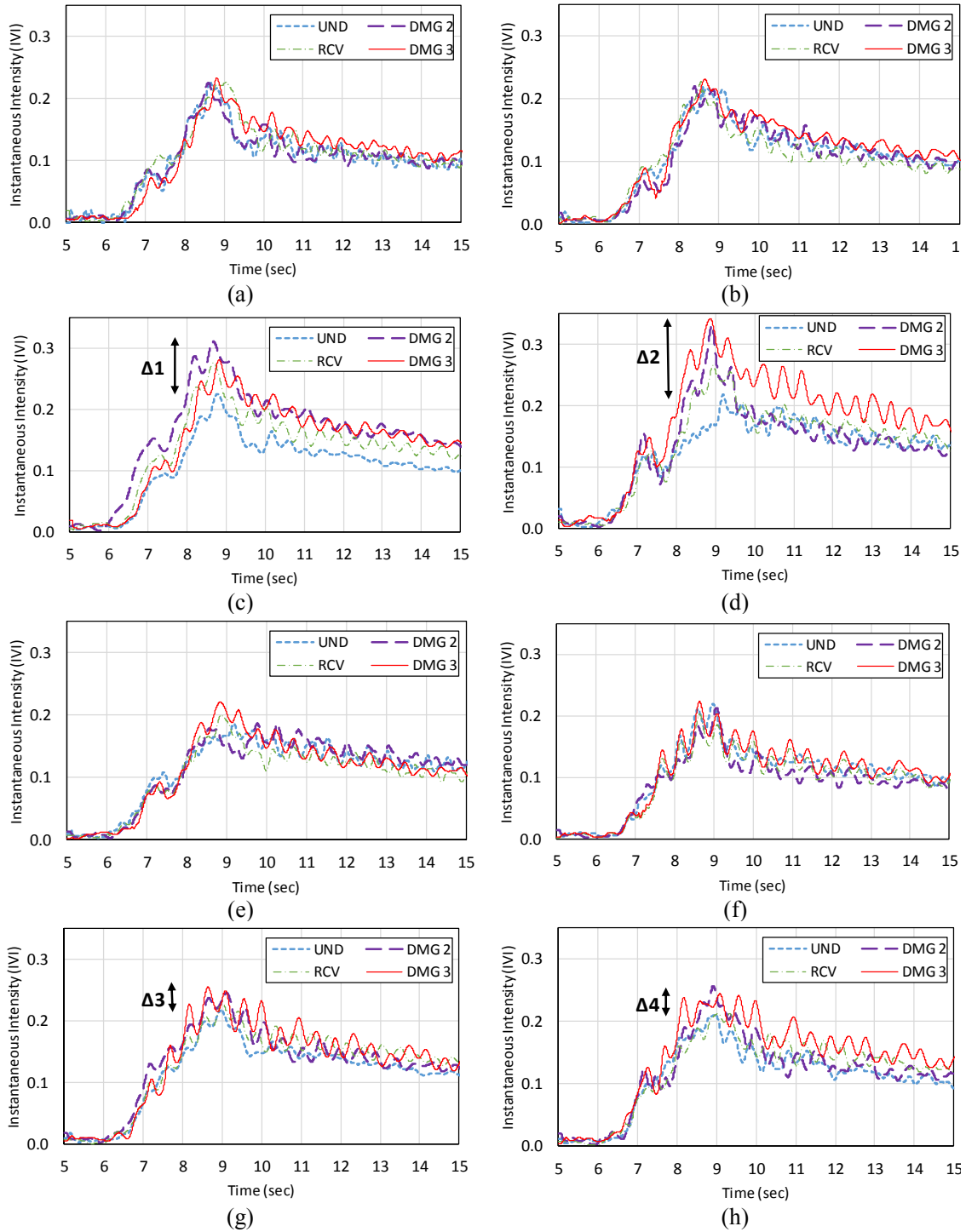
Figure 11. Variation of Instantaneous Vibration Intensity parameter (IVI) for frequency 1 (IMF 3) at each sensor location along the bridge during all damage states: (a) sensor 1 (b) sensor 2 (c) sensor 3 (d) sensor 4 (e) sensor 5 (f) sensor 6 (g) sensor 7 (h) sensor 8.

Further on, Figure 12 (a) and Figure 12 (b) plot the changes of IVI at each sensor considering two damage states (DMG 2 and DMG 3) for the fundamental frequency (IMF

3). In the first case, the sensor 4 obtains a maximum peak of 0.33 and all instantaneous intensities registered by sensor 3 are amplified, which indicates that the damage 2 (DMG 2) occurs in this location as shown in Figure 3. In the second case, it is clearly evident how the intensities in sensor 4 are amplified exactly in the position where the damage 3 occurred (DMG 3). In conclusion, the instantaneous vibration intensity referred to the first vibration frequency is able to identify and locate the damage in the exact position where the sensor is located.
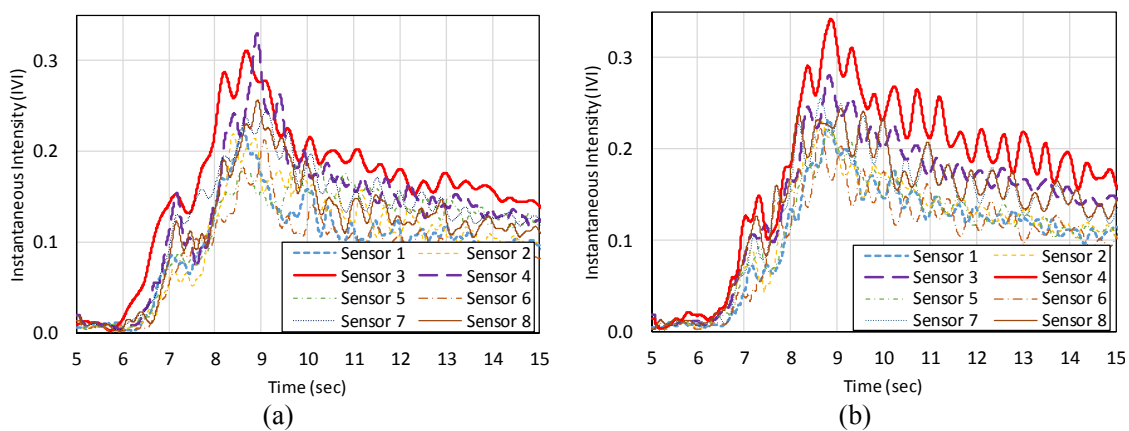
Figure 12. Variation of Instantaneous Vibration Intensity (IVI) parameter for frequency 1 in two damage scenarios: (a) damage 2 (DMG 2) (b) damage 3 (DMG 3).

In this part, the results obtained from the analysis carried out previously are verified, in which IVI parameter obtained good performance to detect and locate the damage in the bridge. Figure 13 shows the analysis of instantaneous frequencies for the most critical sensors 3 and 4 where damage 2 and 3 occurred respectively. Figure 13 (a) shows that the frequency 1 (IMF 3) captured by the sensor 3 has a very clear behavior and the signal does not present noise, whereby this frequency can be correctly identified. In the first case, when the condition of bridge goes from the undamaged state to damage 2 (DMG 2) the average frequency 1 decreases from 3.0 Hz to 2.85 Hz. In the recovered damage scenario, the bridge shows a slight increase in average frequency from 2.85 Hz to 2.95 Hz. Finally, for the most critical damage 3 (DMG 3), the average frequency

decreases from 2.95 Hz to 2.90 Hz. In the present study, good instantaneous frequencies results were obtained in contrast with reference analysis developed by Kim et al. (2014). In the same way, Figure 13 (b) depicts the frequencies obtained in each damage scenario for sensor 4, and it presents the same behavior between undamaged, damaged and recovered bridge condition (e.g. increase and decrease of frequency).
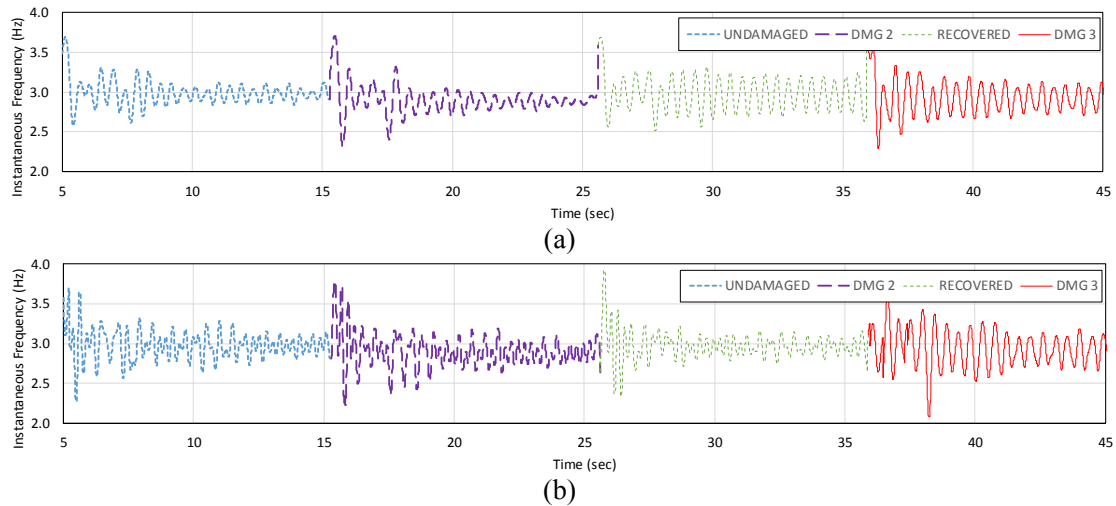

Figure 13. Variation of Instantaneous frequencies 1 (IMF 3) at each damage stages (a) sensor 3 (b) sensor 4.

Additionally, instantaneous amplitude analysis is performed for the most critical sensors 3 and 4 where damage 2 and 3 occurred respectively, this can be shown in Figure 14. For sensor 3, Figure 14 (a) shows that the instantaneous amplitude in the undamaged state (UND) has a maximum peak of 0.62. However, when damage 2 occurs (DMG 2) the maximum peak increases to 0.83 getting a maximum variation of $\Delta 1 = 0.21$. Then, the recovered state of the structure (RCV) occurs when the bridge has a behaviour of returning to its initial state (undamaged). Finally, in the third damage (DMG 3) the maximum amplitude peak increases in value. In the same way, the analysis of the sensor 4 (Figure 14b) shows a similar behaviour like presented in sensor 3, since the damage 3 occurs in location of sensor 4. In addition, in this state, the maximum peak reaches a value of 0.96, which produces a maximum variation of $\Delta 2 = 0.32$.
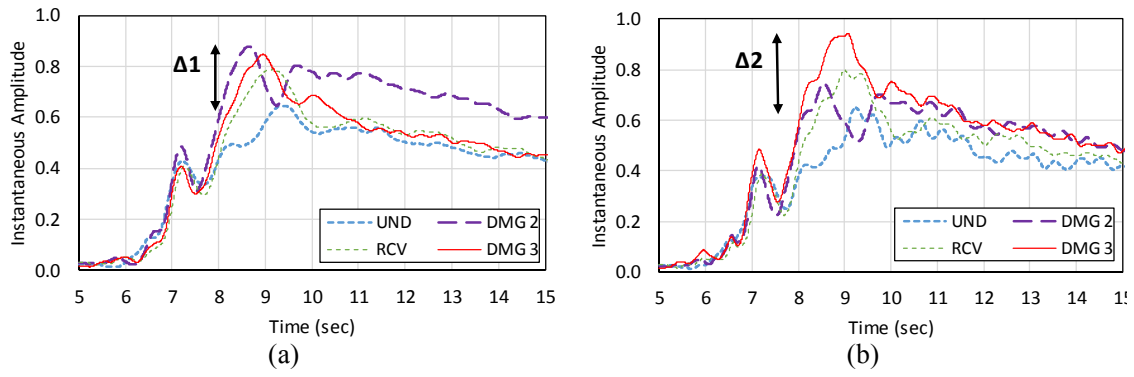
Figure 14. Variation of Instantaneous amplitudes for IMF 3 at each damage stages (a) sensor 3 (b) sensor 4.

On the other hand, Figure 15 (a) to Figure 15 (h) shows the behaviour of IVI in each sensor for the second vibration frequency (IMF 2). In this case, the maximum peaks do not help to identify the damage, nonetheless, when damage occurs the tendency to increase of IVI is maintained. Furthermore, a clear signature of damage is not identified and this could be due to noise presented in frequencies and amplitudes. This is clearly understood since the IVI has a direct relationship with the instantaneous vibration frequencies and amplitudes (as shown in equation 10).
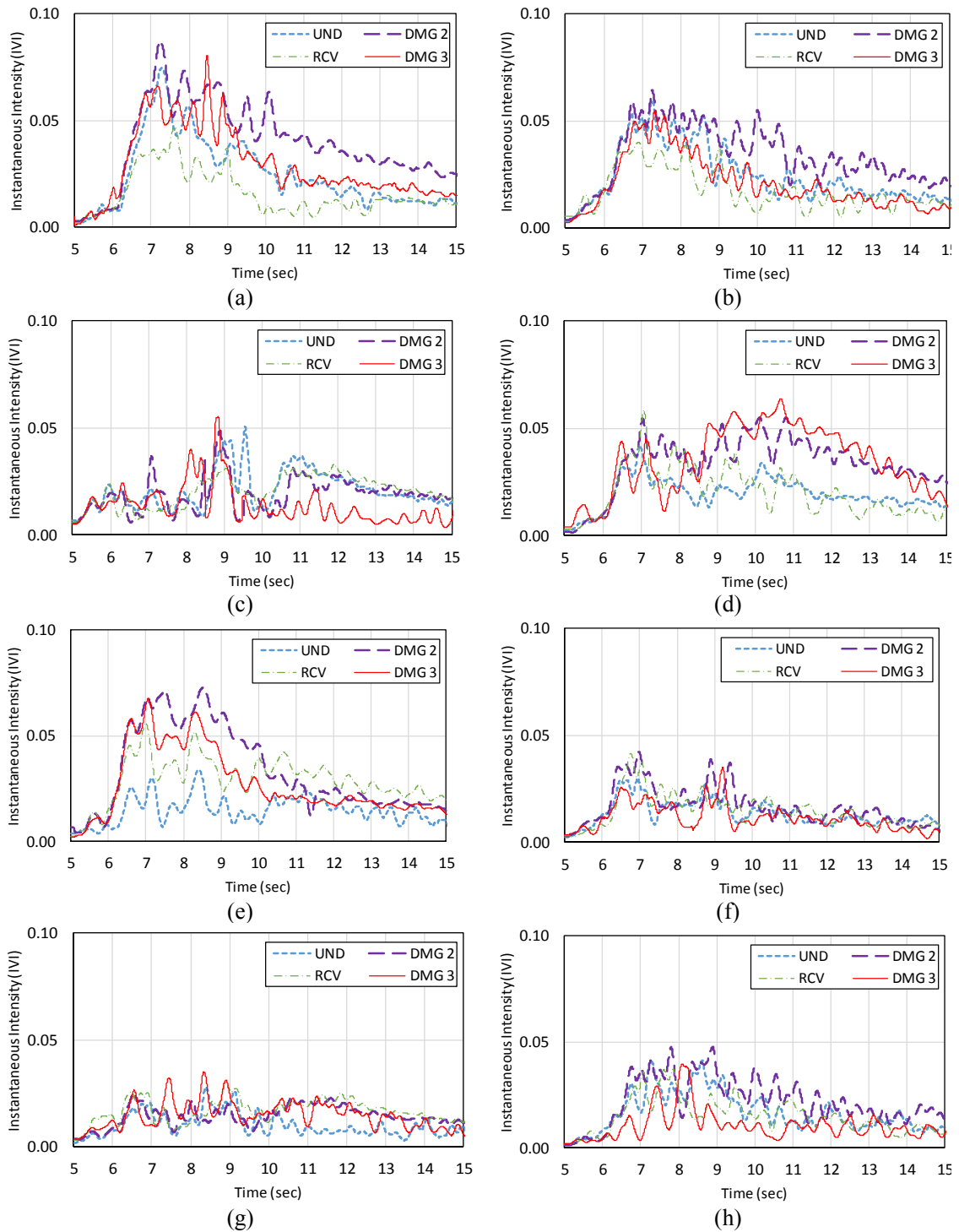
Figure 15. Variation of Instantaneous Intensity parameter (IVI) for frequency 2 (IMF 2) at each sensor locations along the bridge during all damage states: (a) sensor 1 (b) sensor 2 (c) sensor 3 (d) sensor 4 (e) sensor 5 (f) sensor 6 (g) sensor 7 (h) sensor 8.

Figure 16 (a) and (b) provide the variation of the instantaneous frequency 2 (IMF 2) for the most critical sensors 3 and 4 respectively. In this regard, both sensors can not

be used to identify the presence of structural damage over time. In the same way, this behaviour does not represent the physical condition of the four damage scenarios already studied. In conclusion, the second frequency of vibration (IMF 2) is not able to recognize the structural damage due to the presence of high noise level in the signals.
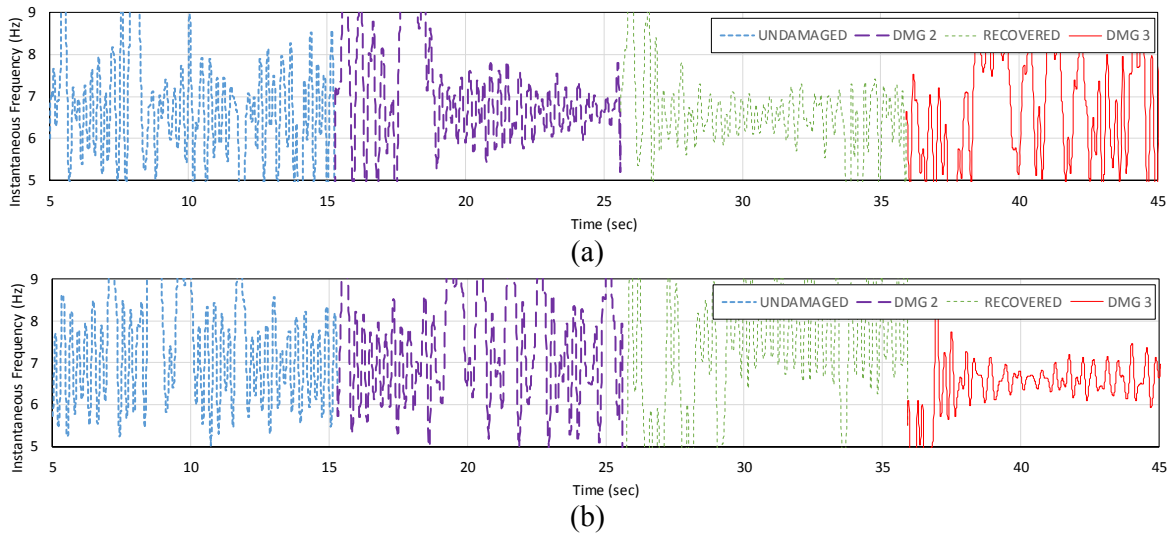
Figure 16. Variation of Instantaneous frequencies 2 (IMF 2) at each damage stages (a) sensor 3 (b) sensor 4.

The study of the instantaneous amplitude for the second vibration frequency is shown in Figures 17 (a) and (b) for sensors 3 and 4 respectively. Taking as reference that the IVI parameter depends on the instantaneous amplitude, it is verified that this is not useful to identify and locate the damage because in both cases there is no maximum reference peak, furthermore, there is no trend that can be useful for evaluate the undamaged and damaged condition of the bridge.
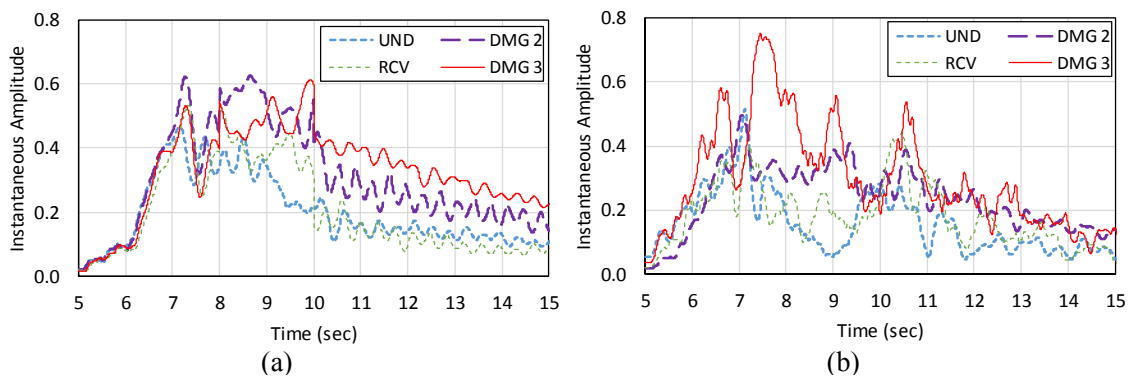
Figure 17. Variation of Instantaneous amplitudes for IMF 2 at each damage stages (a) sensor 3 (b) sensor 4.

In the same way, the instantaneous intensity related to the fifth vibration frequency (IMF 1) is shown from Figure 18 (a) to Figure 18 (h) for all sensors. The results show that the IVI parameter does not present a well-established damage feature and presents a high variability. For this reason, the exact position of the damage can not be located. Bearing in mind the same analysis for IMF 2, Figure 19 and Figure 20 plot the instantaneous frequency and amplitude respectively. Thereby, the IVI parameter from IMF1 can not be used to identify the damage because the frequencies as well as amplitudes are highly variable.
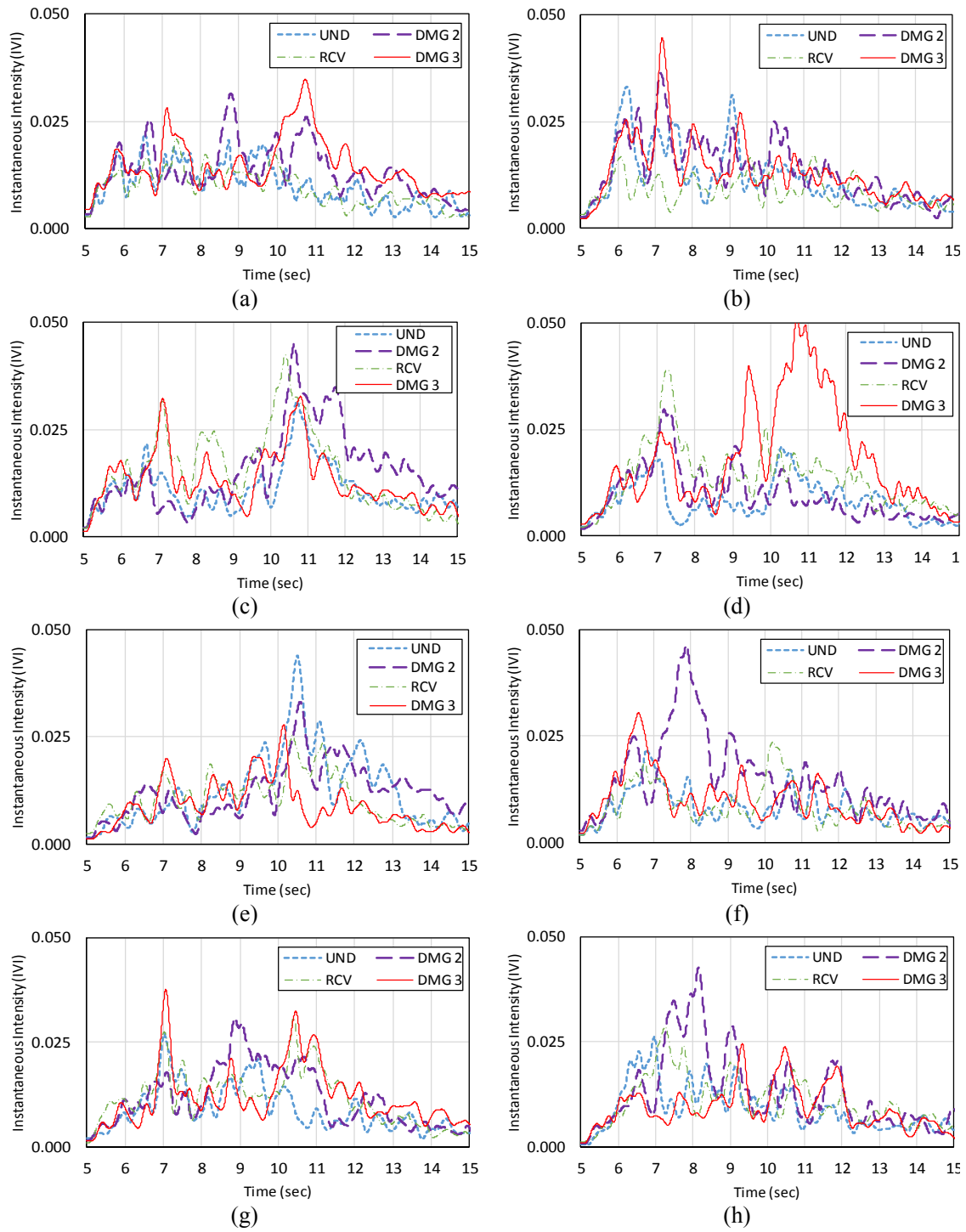
Figure 18. Variation of Instantaneous Intensity parameter (IVI) for frequency 5 (IMF 1) at each sensor locations along the bridge during all damage states: (a) sensor 1 (b) sensor 2 (c) sensor 3 (d) sensor 4 (e) sensor 5 (f) sensor 6 (g) sensor 7 (h) sensor 8.
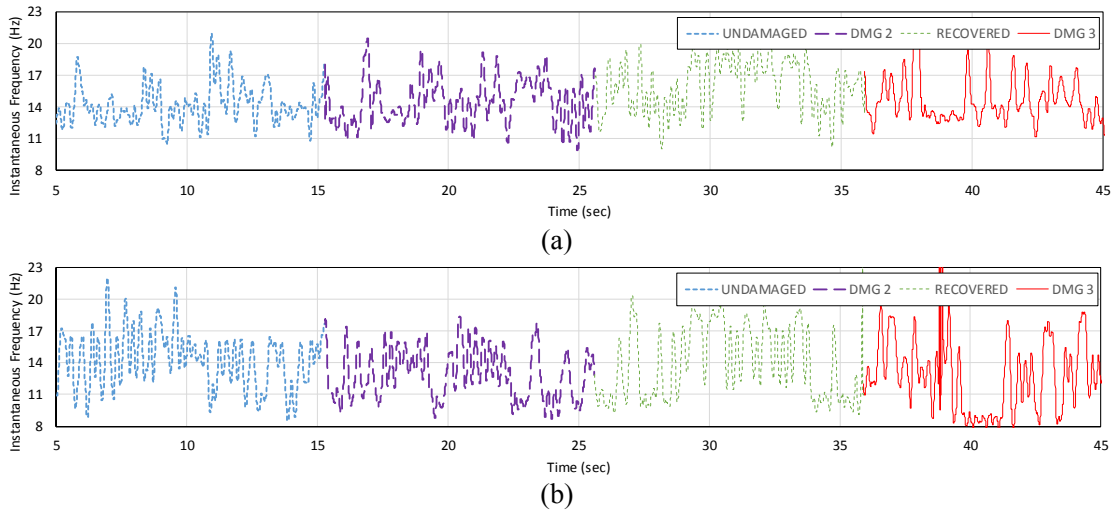
Figure 19. Variation of Instantaneous frequencies 2 (IMF 1) at each damage stages (a) sensor 3 (b) sensor 4.
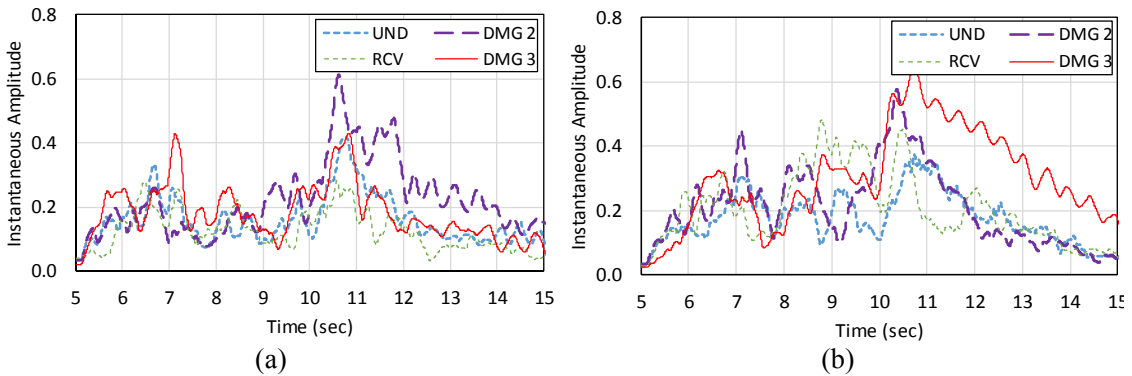

Figure 20. Variation of Instantaneous amplitudes for IMF 1 at each damage stages (a) sensor 3 (b) sensor 4.

As a conclusion of this analysis, only the case of IMF 3, corresponding to the first vibration mode, reported accurate results regarding detection and location of damage.

5.2.2 Analysis based on total IMF (AIVI)

The approach of this study also includes a more complete and deep analysis to the one presented by (Moughty & Casas, 2018a). For this purpose, a further analysis of instantaneous vibration intensity is performed in order to detect and locate the damage on the bridge. Thus, the IVI parameter is modified in the Amalgamated Instantaneous Vibration Intensity (AIVI) which uses the combination of the detected IMFs of the first,

third and fifth natural frequencies. In addition, the influence of different damages on all sensors are considered and studied.

Figure 21 shows the variation of AIVI parameter over time. For instance, sensor 1 (Figure 21a) shows normal behavior in all four damage scenarios and this can be verified because imposed damage was far away. A similar behavior was found in sensors 2, 5 and 6 as shown in Figure 21 (b), Figure 21 (e) and Figure 21 (f) respectively. However, taking into account the undamaged state of the bridge as reference, in Figure 20(c) the sensor 3 presents a slight variation ($\Delta 1=0.03$) caused by the total cut in a vertical member at 5/8th-span (DMG 2). Furthermore, the maximum damage was identified (DMG 3) for sensor 4 as shown Figure 21 (d) and this is presented in the large increase of AIVI parameter ($\Delta 2=0.12$) that clearly reflects the severity and intensity of the damage, and in this way, it can be measured and compared with the rest of the sensors. Moreover, Figure 20(g) and Figure 21 (h) display a slight increase of AIVI parameter in the location of the sensors 7 and 8 due to the damages 2 and 3 respectively. For damage 2, the sensor 7 is able to capture a variation of $\Delta 3=0.02$ and sensor 8 increases in intensity by a value of $\Delta 4=0.04$ because of damage 3. This slight variation can be explained since sensors 7 and 8 are located in front of sensors 3 and 4 taking as reference the cross section of the bridge (as shown in Figure 3). In this way the value of AIVI becomes only slightly modified because the damage is not close to them.
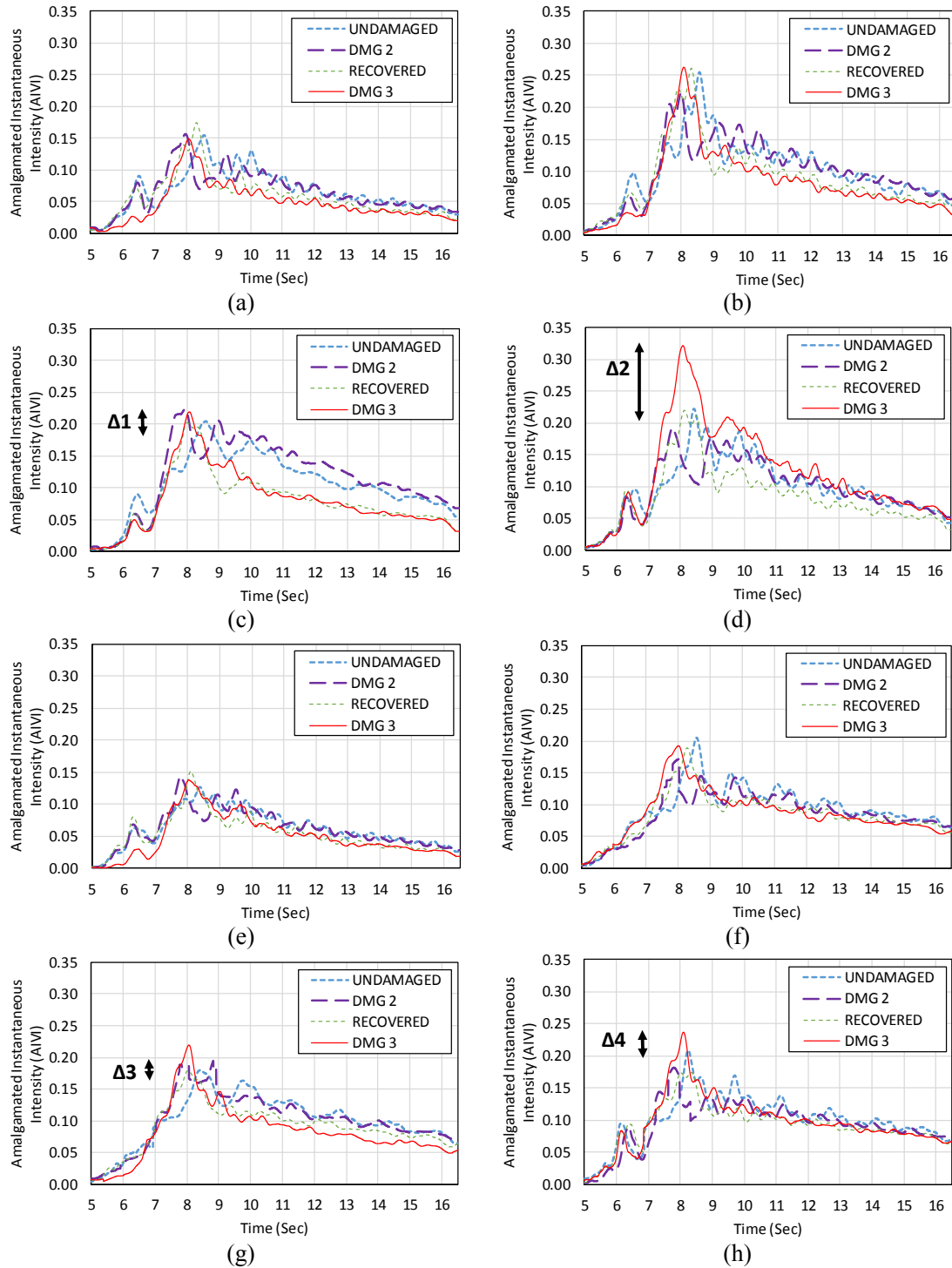
Figure 21. Vertical variation of Amalgamated Instantaneous Vibration Intensity (AIVI): (a) sensor 1 (b) sensor 2 (c) sensor 3 (d) sensor 4 (e) sensor 5 (f) sensor 6 (g) sensor 7 (h) sensor 8.

Figure 22 (a) and Figure 22 (b) show the behavior of the most critical positions: sensor 3 and 4 on one side and sensor 7 and 8 on the other side of the bridge. In this case,

the evolution of the intensity over time indicates that the damage and the recovery can be detected automatically and AIVI vibration parameter improves the sensitivity to the detection of damage when compared to the results obtained with IVI in the previous section. Finally, all the sensors captured the recovery behaviour (RCV scenario) and this is shown when the AIVI values try to return to the undamaged state.
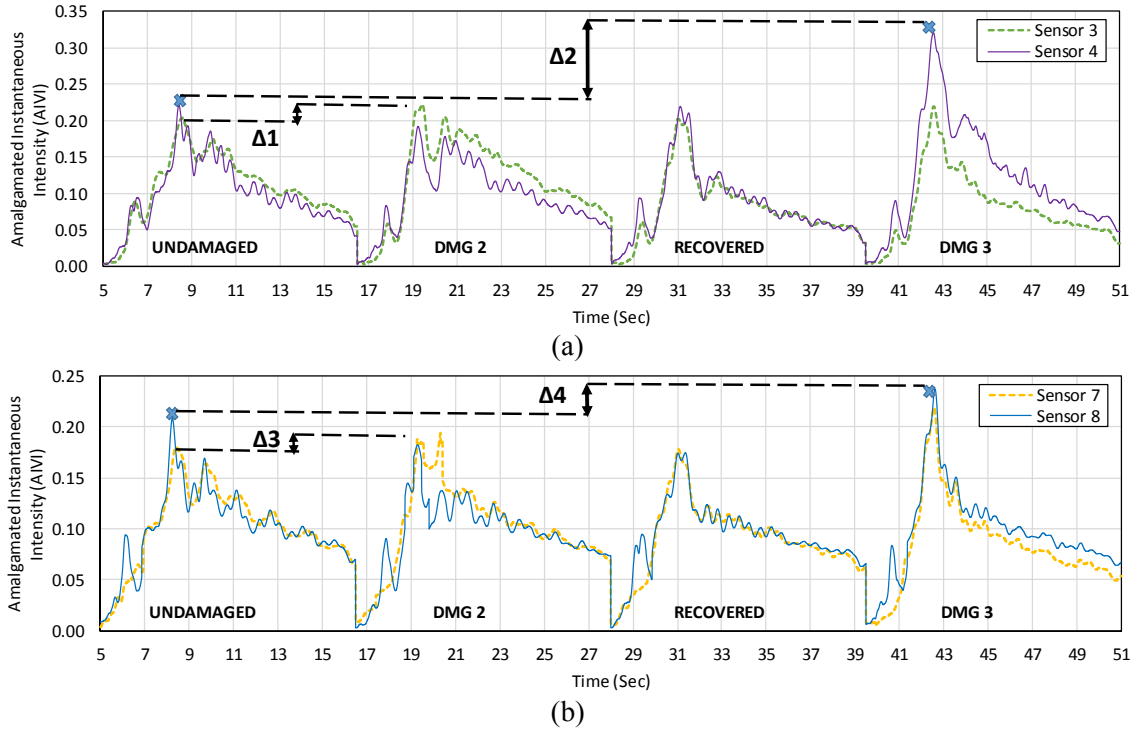

Figure 22. Comparison of AIVI parameter between critical sensors located in the damages: (a) sensor 3 and sensor 4 (b) sensor 7 and sensor 8.

The present study expands this inquiry to show the different phases of AIVI variation during the excitation time induced by the vehicle. For this purpose, Figure 23 (a) shows stationary values of all sensors for initial undamaged condition (IP1=Initial Position). This state displays a maximum value aligned for all sensors in 8.6 seconds. Besides, in forced vibration time interval, a larger instantaneous intensities induced by the vehicle passage could be observed. The instantaneous values are significantly higher for damaged cases compared with the undamaged state (healthy) bridge structure. In the beginning (5-8.6 s approximately), the Figure 23 (b) plots the AIVI values for damage

level 2 which increase relatively (DMG 2) and these were moved to the left compared with undamaged state. All the sensors show that maximum intensity values are shifted to the left 1 second approximately, from the initial position (IP1) to the final position (FP1). This behaviour is observed after the vehicle has passed over the sensor 3 location, where the second damage occurred (DMG 2). Figure 23 (c) provides the recovery state (RCV). The maximum peaks of instantaneous intensity try to move to the right from a final position (FP1) to another final position (FP2). From this behaviour, it can be understood that bridge structure attempts to return to its undamaged initial condition. Afterwards, as shown in Figure 23 (d), the tendency of the peaks is to move to the left. This is reasonable since in this scenario the greatest damage occurred (DMG 3) and the most critical sensor 4, unlike others, suffers significant changes of AIVI due to damage occurring in this position. The maximum peaks move to the left from a final position (FP2) to another final position (FP3) and the time shift is around 0.5 seconds.

As a final caveat, a maximum increase of 0.2 to 0.32 in AIVI parameter was obtained during 1 second approximately, it could be recognized after all the damage scenarios imposed to bridge structure. All this behaviour of induced excitation in the bridge can be understood because for each damage scenario, the forced vibration data that the vehicle generated were taken as the average between the three passages at 40km/h approximately.
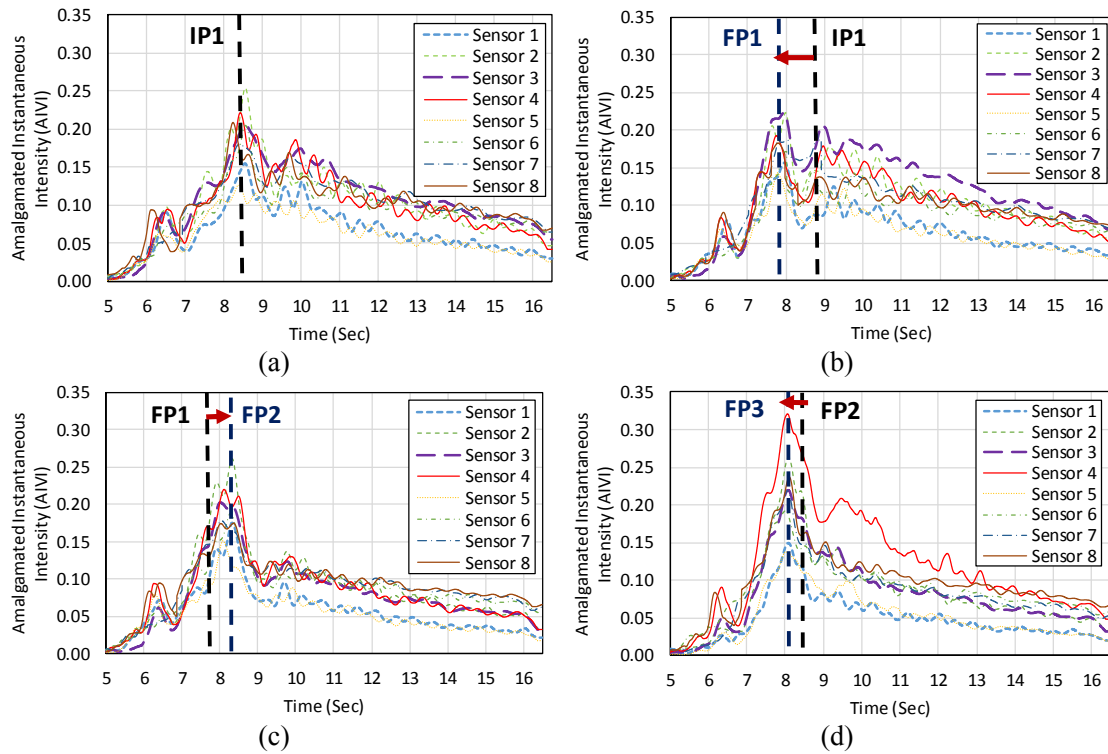
Figure 23. Maximum peak variation in four damage scenarios over time of AIVI parameter (a) undamaged (UND) (b) damage 2 (DMG 2) (c) recovered (RCV) (d) damage 3 (DMG 3).

For more detail, the present study also suggests to consider other damage feature parameters that can be extracted from Amalgamated Instantaneous Vibration Intensity. Figure 24 shows a second maximum point candidate to analyse structural damages. In this case, the pattern of the AIVI parameter is similar to the one presented in Figure 23. According to Figure 24 (a), the second maximum point is located at 9.9 seconds for undamaged condition. Then, second peaks follow a well-known trend, these move from right to left (IP1 to FP1) due to first damage like can be seen in Figure 24 (b). After that, the bridge structure recovers and attempts to return to its initial state of undamaged condition (Figure 24c). Furthermore, the final position (IP1) moves to another final position (FP2). Subsequently, the Figure 24(d) plots the extreme scenario for damage DMG 3 where the amalgamated instantaneous intensity goes to final position (FP3), and

this final state shows clearly a higher variation that exists in the AIVI parameter captured by all the sensors.

Therefore, the horizontal and vertical changes experienced by Amalgamated Instantaneous Vibration Intensity parameter (AIVI) serve to identify and locate the damage in the bridge, and this trend improves when the maximum peaks are analysed in detail. It is shown that AIVI (all IMF´s together) is a better suited parameter for damage identification than IVI (IMF´s separately). The results obtained by (Chang & Kim, 2016), when analysing the same test but in the free vibration part of the acceleration signal, are similar to the ones obtained here. In fact, in their study the analysis based on a single frequency was as effective as when using multiple ones, because it was sensitive only to certain specific damage scenarios. Therefore, AIVI will be used in the next section to compare its performance with the other selected parameters in the case of forced vibration.
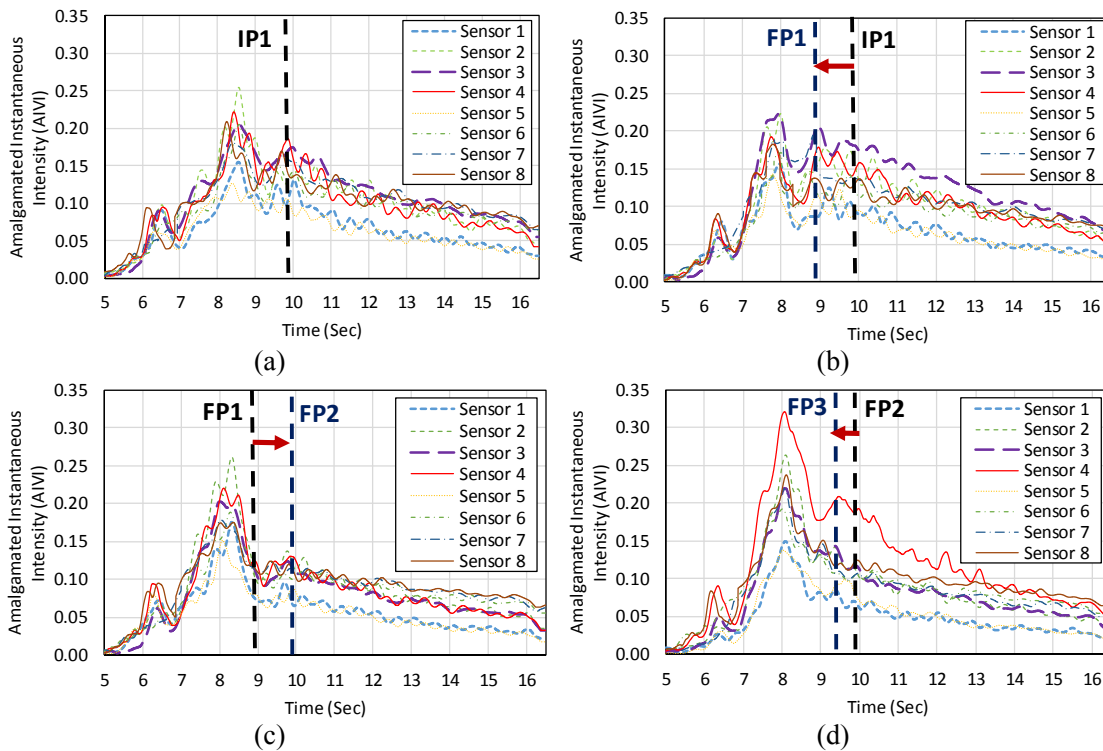

(a)

(b)

(c)

(d)

Figure 24. Second peak variation of AIVI parameter in four damage scenarios over time (a) undamaged (UND) (b) damage 2 (DMG 2) (c) Recovery (RCV) (d) damage 3 (DMG 3).

5.2.3 Comparison of vibration parameters from forced vibrations

The damage identification assessment results for the Steel Truss Bridge under vehicle induced excitation are presented herein for the three vibration parameters that were deemed suitably applicable to such conditions as per the criteria set out in Table 2: CAV, CAD and AIVI. In addition, a damage indicator parameter is employed to quantify the changes per sensor per damage scenario. This is called Cumulative Difference Ratio (CDR) as presented in (Moughty & Casas, 2018a). CDR is presented in Equation (13), in the case of parameter AIVI, where $\sum_{i=1}^{n}\left(AIVI_{Dami}\right)$ and $\sum_{i=1}^{n}\left(AIVI_{UDi}\right)$ are the cumulatively summed values of AIVI across time for the damaged state and undamaged state, respectively. A similar equation applies in the case of CAV and CAD.

$$CDR(\%) = \frac{\sum_{i=1}^{n}\left(AIVI_{Dami}\right) - \sum_{i=1}^{n}\left(AIVI_{UDi}\right)}{\sum_{i=1}^{n}\left(AIVI_{UDi}\right)} x100 \qquad (13)$$

(1) CAV

Figure 25 presents the CAV values obtained at all 8 sensor locations (as per Figure 3) for the condition states of; Undamaged, DMG2, RCV & DMG3. All values are normalized to the largest undamaged value. It is evident from Figure 24(d) that the DMG3 condition yields a significant change in CAV at Sensor 4, which is the damage location. However other condition states are less separable by eye. For this reason, Figure 26 is used to portray the percentage variation from baseline for sensors 1-5 for DMG2, RCV & DMG3. From here it is clearer that the spikes associated with DMG2 & DMG3 are located at the point of damage, while the percentage variation of the RCV state is less pronounced,

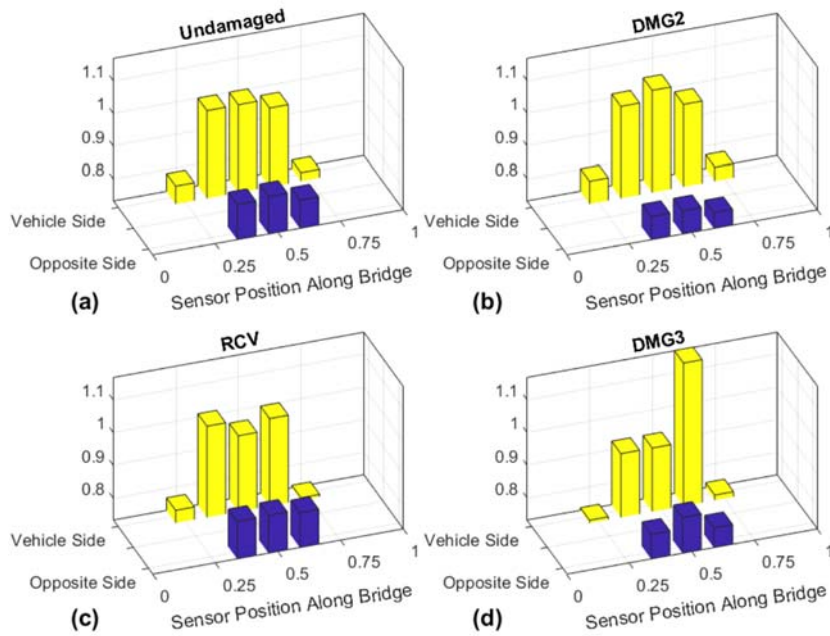indicating that the recovery process succeeded in realigning bridge behavior to near baseline.

Figure 25. Normalized CAV values per sensor for damage scenarios; (a) Undamaged, (b) DMG2, (c) RCV & (d) DMG3.
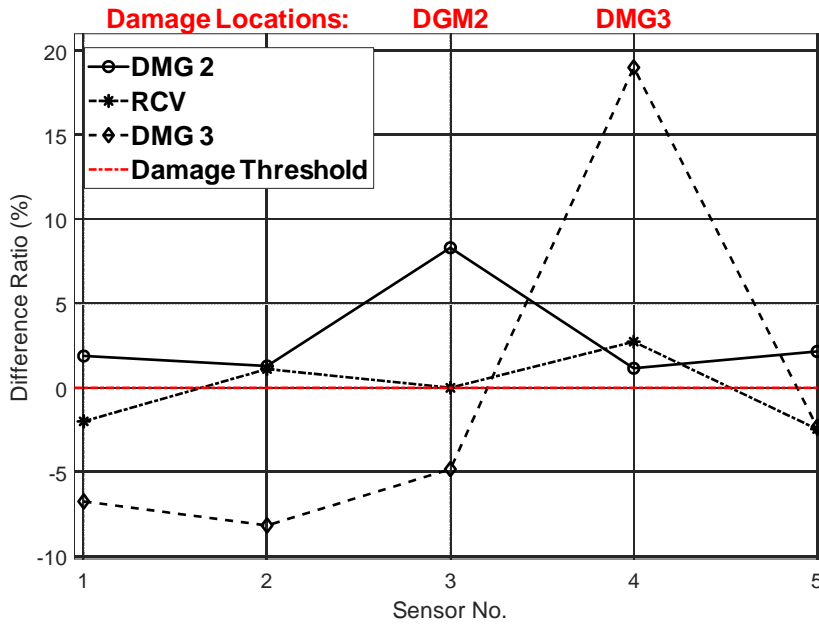

Figure 26. CAV percentage variation from baseline at sensors 1-5 for damage scenarios; DGM2, RCV & DMG3.

(2) CAD

Figure 27 presents the CAD values obtained at all 8 sensor locations (as per Figure 4.) for the condition states of; Undamaged, DMG2, RCV & DMG3. All values are normalized to the largest undamaged value. Again, it is clear that DMG3 yields a significant change in CAD at Sensor 4, which is the location of damage. In Figure 28, the percentage variation from baseline for sensors 1-5 for DMG2, RCV & DMG3 is given, which shows clear damage at sensors 3 & 4 for damage states DMG2 & DMG3, respectively. Both sensors are located at the point of damage, indicating a successful damage location assessment. Furthermore, the RCV state is close to baseline, which correctly indicates no damage present.
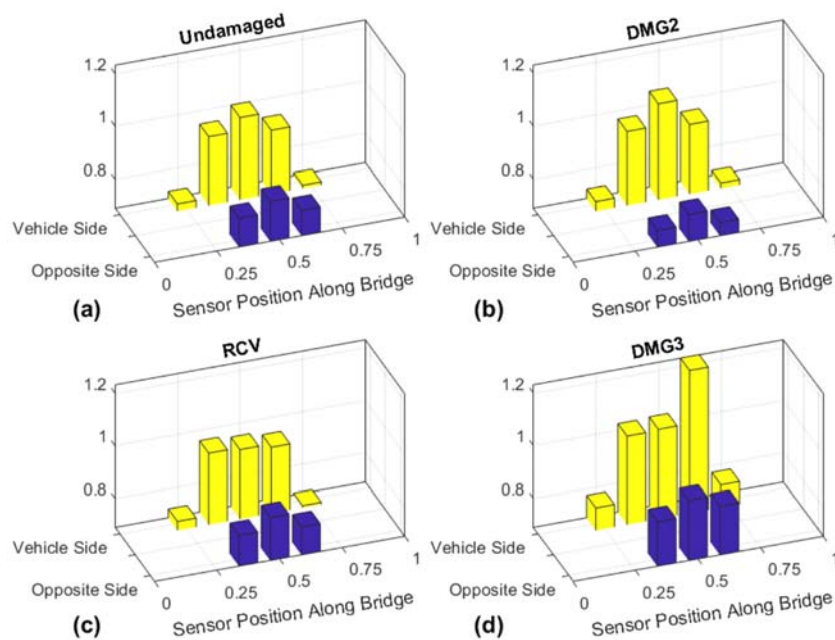

Figure 27. Normalized CAD values per sensor for damage scenarios; (a) Undamaged, (b) DMG2, (c) RCV & (d) DMG3.
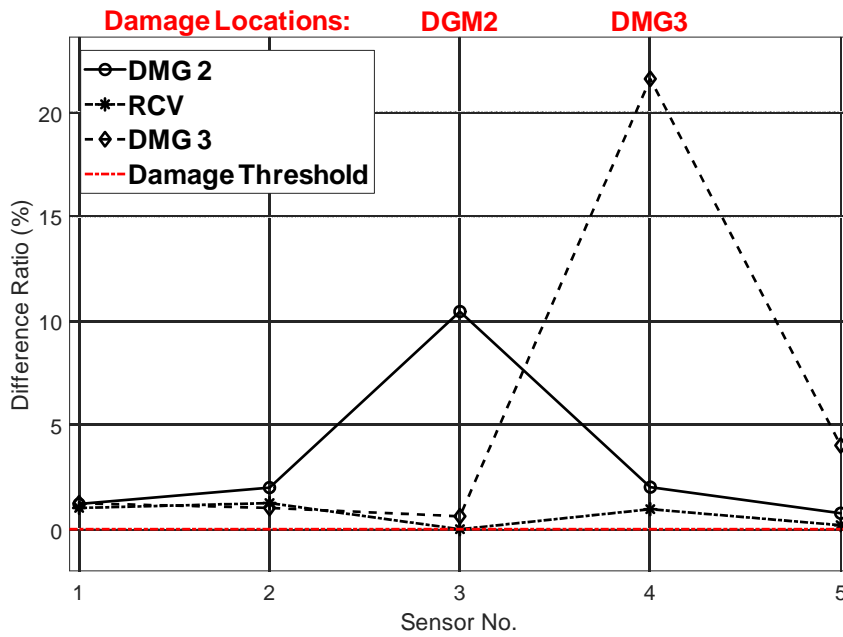
Figure 28. CAD percentage variation from baseline at sensors 1-5 for damage scenarios; DGM2, RCV & DMG3.

(3) AIVI

Figure 29 presents the AIVI values obtained at all 8 sensor locations (as per Figure 4.) for the condition states; Undamaged, DMG2, RCV & DMG3, of which, DMG3 is again the most obvious divergent. The percentage variation of sensors 1-5 is presented in Figure 30 for the condition states of; DMG2, RCV & DMG3. It is evident that the two damage locations are identified by AIVI, those being sensors 3 and 4 for condition states DMG2 & DMG3, respectively.
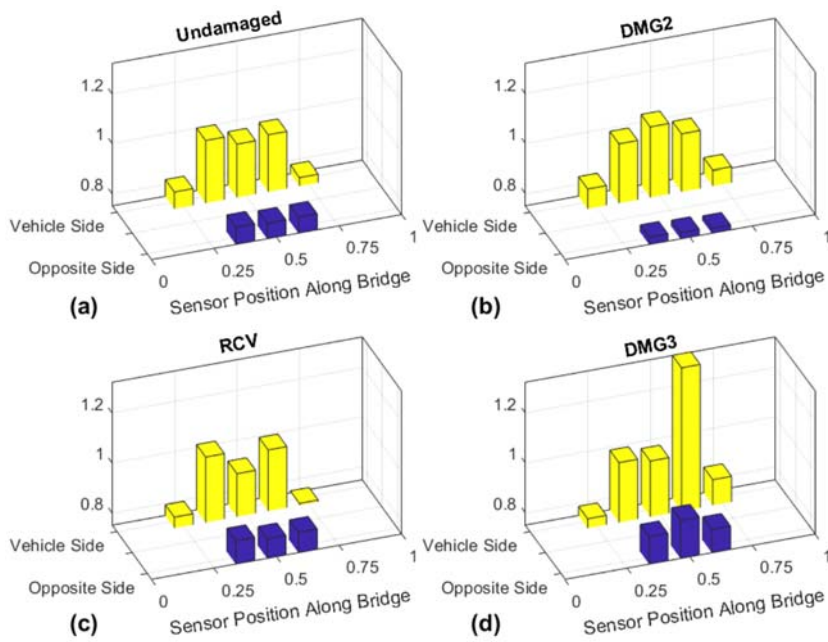
Figure 29. Normalized AIVI values per sensor for damage scenarios; (a) Undamaged, (b) DMG2, (c) RCV & (d) DMG3.
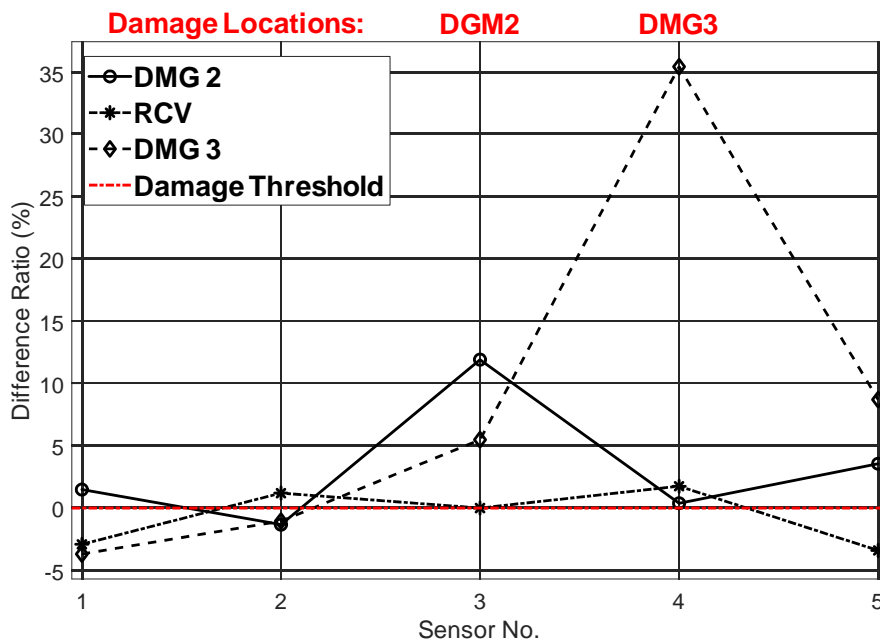

Figure 30. AIVI percentage variation from baseline at sensors 1-5 for damage scenarios; DGM2, RCV & DMG3.

6 DISCUSSION

Based on the results of the present study, some recommendations for practical cases and advice for practitioners on the best method to use depending on the characteristics of the recorded data are presented in Figure 31 and discussed herein.

1. In the ambient induced excitation case study, two methods of outlier detection were employed; MSD for the Gaussian distributed parameters DVI & MCVI, and Euclidian Distance of the symbolic data objects from the LogNormal distribution of the energy based CAV. Of the three parameters assessed, CAV portrayed the strongest indication of damage for the pier settlement test, while DVI was able to identify both types of damage, pier settlement and simulated stiffness loss.

2. In the vehicle induced excitation case study, all empirical vibration parameters assessed (CAV, CAD, IVI & AIVI) identified the required damage events, with CAD providing the greatest resolution regarding the damage location, as displayed by the singular spikes in Figure 27.

3. The parameters based on vibration energy showed significant increase throughout the time range for all sensors close to damage. In contrast with a sensor away from undamaged state, where no appreciable change in vibration magnitudes were observed with increasing levels of damage.

4. To evaluate the damage using the AIVI parameter, it is not only necessary to find the maximum peak points, but it is important to analyse the behaviour of the intensity during the entire time of the forced load test. According to the exhaustive evaluation of instantaneous intensity, the first fundamental frequency, unlike the second and fifth, is the one that obtained better and clear results to identify and locate the damage on the bridge.

5. To evaluate the damage identification capability of the vibration parameters assessed under vehicle induced excitation, the percentage variation observed at

the damage location for condition states; DMG2, RCV & DMG3 are given in Table 5 and can be compared against modal frequency changes for each damage scenario in Table 6, courtesy of Kim et al. (2014). From the comparison, all of the vibration parameters assessed appear to outperform the modal frequency changes in this regard, with AIVI's percentage differences producing the best overall.
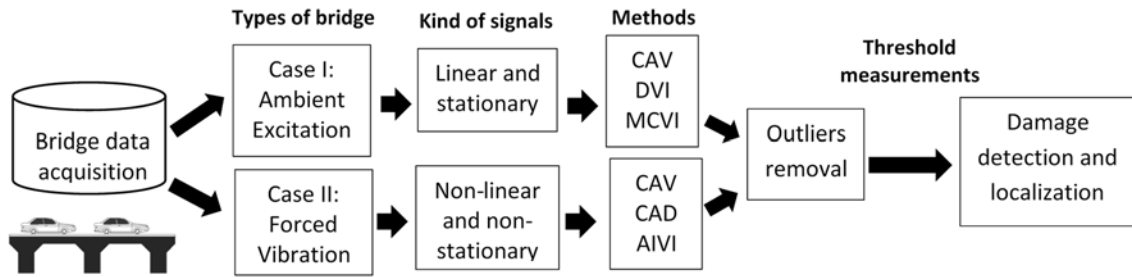

Figure 31. Flowchart to choose the most appropriate method in the damage identification.

Table 5. Vibration parameter variation for total number of sensors and damage scenarios

Vibration Parameter	DMG2	RCV	DMG3
CAV	+9.1%	+0.1%	+19.8%
CAD	+10.2%	-0.1%	+22.2%
AIVI	+12.3%	-0.1%	+35.8%

Table 6. Modal frequency variation (Kim et al., 2014)

Mode	DMG2	RCV	DMG3
1st B. Mode	-2.67%	-0.13%	+0.31%
2nd B. Mode	+0.20%	-0.25%	-5.67%
3rd B. Mode	-0.21%	-0.87%	-9.05%
4th B. Mode	+0.22%	-0.72%	-6.87%
5th B. Mode	+0.58%	+0.19%	-0.16%

6 CONCLUSIONS

The present paper describes a set of novel vibration parameters such as CAV, CAD, DVI, MCVI, IVI and AIVI and their feasibility as damage features to detect damage using ambient and forced vibrations in two real bridges. Bridge data can be obtained from ambient or forced vibration, that at the same time may present some particularities such as linearity and stationarity. For instance, in the first bridge analyzed, the signals are linear

and stationary, however in the second case, the bridge is subjected to a forced vibration, which produces non-linear and non-stationary signals. The developed strategy consists of using non-modal vibration-based methods. The results presented in this paper, have demonstrated that many of the novel empirical vibration parameters assessed are suitable for damage identification (detection, localization & quantification), provided that they are applied to a suitably applicable vibration signal type, as per the criteria set out in Table 1 and Figure 31, and provided that a suitable outlier detection method is chosen based on the distribution type of the extracted vibration parameter. Some practical recommendations for application of the proposed techniques are listed in the discussion section.

However, it should be pointed out that in both bridge data analysed, operational and environmental effects are not considered in the present study. To include those effects in the damage detection performance of the defined vibration parameters is the subject of further research.

8 REFERENCES

Colominas, M.A., Scholtthauer, G., & Torres, M.E. (2014). Improved complete ensemble EMD: A suitable tool for biomedical signal processing. *Biomedical Signal Processing and Control*, 14, 19–29.

Chang, K.C., & Kim, C.W. (2016). Modal-parameter identification and vibration-based damage detection of a damaged steel truss bridge. *Engineering Structures*, 122, 156–173.

Ding, K., & Chen, T. P. (2013). Study on Damage Detection of Bridge Based on Wavelet Multi-Scale Analysis. In *Advanced Materials Research* (Vol. 639, pp. 1010-1014). Trans Tech Publications.

Fassois, S. D., & Kopsaftopoulos, F. P. (2013). Statistical time series methods for vibration based structural health monitoring. In *New trends in structural health monitoring* (pp. 209-264). Springer, Vienna.

Goi, Y., & Kim, C. W. (2017). Damage detection of a truss bridge utilizing a damage indicator from multivariate autoregressive model. *Journal of Civil Structural Health Monitoring*, 7(2), 153-162.

Huang, N. E., Long, S. R. & Shen, Z. (1996). The mechanism for frequency downshift in nonlinear wave evolution. In *Advances in applied mechanics* (Vol. 32, pp. 59-117C). Elsevier.

Hester, D., & González, A. (2012). A wavelet-based damage detection algorithm based on bridge acceleration response to a vehicle. *Mechanical Systems and Signal Processing*, 28, 145-166.

Kankanamge, L., & Dhanapala, Y. S. S. (2016). Application of Wavelet Transform in Structural Health Monitoring.

Kim, C.W., Kitauchi, S. & Sugiura, K. (2013). Damage detection of a steel bridge through on-site moving vehicle experiments. In *Proceedings of the Second Conference on Smart Monitoring, Assessment and Rehabilitation of Civil Structures (SMAR2013), Istanbul, Turkey*.

Kim, C.W., Chang, K.C., Kitauchi, S., McGetrick, P.J., Hashimoto, K. & Sugiura K., (2014). Changes in modal parameters of a steel truss bridge due to artificial damage. *Safety, Reliability, Risk and Life-Cycle Performance of Structures and Infrastructures- Proceedings of ICOSSAR, New York,* 16-20.

Kramer, S. L. (1996). *Geotechnical Earthquake Engineering*. Prentice-Hall, Upper Saddle River, New Jersey.

Laory, I., Trinh, T. N., Posenato, D., & Smith, I. F. (2013). Combined model-free data-interpretation methodologies for damage detection during continuous monitoring of structures. *Journal of Computing in Civil Engineering*, 27(6), 657-666.

Moughty, J. J. & Casas, J. R. (2017). A state of the art review of modal-based damage detection in bridges: development, challenges, and solutions. *Applied Sciences,* 7(5), 510.

Moughty, J.J. and Casas, J.R. 2018a, Damage Identification of Bridge Structures using the Hilbert-Huang Transform. In *Life Cycle Analysis and Assessment in Civil Engineering: Towards an Integrated Vision: Proceedings of the Sixth International Symposium on Life-Cycle Civil Engineering (IALCCE 2018), 28-31 October 2018, Ghent, Belgium* (pp. 1-8). CRC Press.

Moughty, J.J. & Casas, J.R. 2018b. Noninvasive Empirical Methods of Damage Identification of Bridge Structures using Vibration Data. In *Life Cycle Analysis and Assessment in Civil Engineering: Towards an Integrated Vision: Proceedings of the Sixth International Symposium on Life-Cycle Civil Engineering (IALCCE 2018), 28-31 October 2018, Ghent, Belgium* (pp. 1-8). CRC Press.

Nguyen, V. H., Mahowald, J., Maas, S., & Golinval, J. C. (2014a). Use of time-and frequency-domain approaches for damage detection in civil engineering structures. *Shock and Vibration, 2014*.

Nguyen, T., Chan, T. HT., & Thambiratnam, D. P. (2014b). Controlled Monte Carlo data generation for statistical damage identification employing Mahalanobis squared distance. *Structural Health Monitoring*, 13(4), 461-472.

Ou, Y., Chatzi, E. N., Dertimanis, V. K., & Spiridonakos, M. D. (2017). Vibration-based experimental damage detection of a small-scale wind turbine blade. *Structural Health Monitoring,* 16(1), 79-96.

Rousseeuw, P. J., & Driessen, K. V. (1999). A fast algorithm for the minimum covariance determinant estimator. *Technometrics*, 41(3), 212-223.

Santos, J., Cremona, C., Orcesi, A., & Silveira, P., (2013). Baseline-free real-time novelty detection using vibration-based symbolic features. *Experimental Vibration Analysis for Civil Engineering Structures (EVACES), 28-30 October, Ouro, Brazil.*

Sun, Z., Nagayama, T., Su, D., & Fujino, Y. (2016). A damage detection algorithm utilizing dynamic displacement of bridge under moving vehicle. *Shock and Vibration, 2016.*

Tondreau, G., & Deraemaeker, A. (2014). Automated data-based damage localization under ambient vibration using local modal filters and dynamic strain measurements: Experimental applications. *Journal of sound and vibration*, 333(26), 7364-7385.

Vienna Consulting Engineers, V.C. (2009). *Progressive Damage Test S101 Flyover Reibersdorf* (Report No. 08/2308). Vienna, Austria.

Zhou, Y.-L., Figueiredo, E., Maia, N., Sampaio, R. & Perera, R. (2015). Damage detection in structures using a transmissibility-based Mahalanobis distance. *Structural Control and Health Monitoring*, 22(10), 1209-1222.